

---

## **APPENDIX 2-B: FIGURES**

---

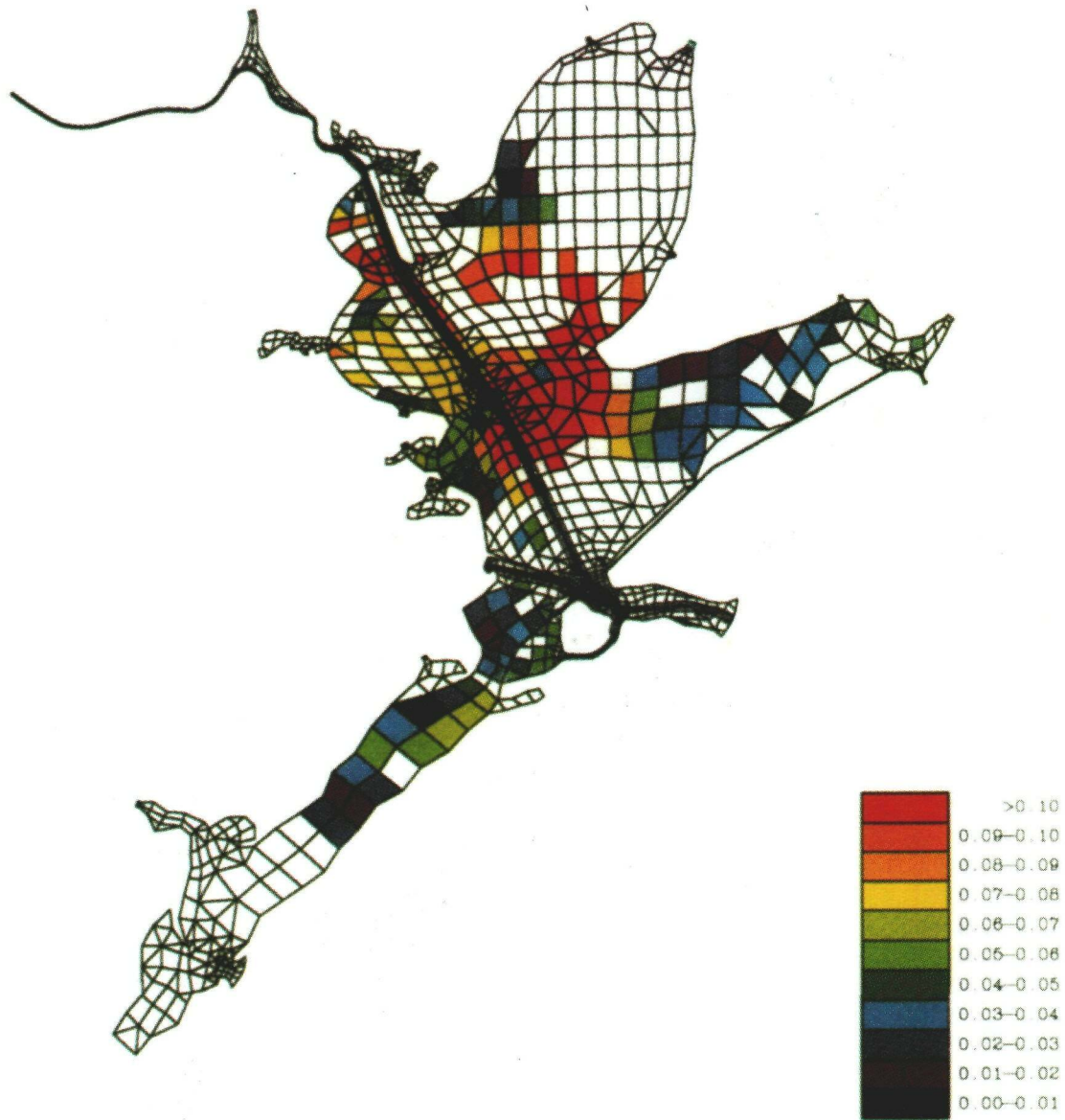


Figure 1. Estimated distribution of shell ( $l\ m^{-2}$ ) obtained using the 51 known sites to predict the values at all unsampled locations and a close-up of the estimated distribution of shell along the Houston Ship Channel. The grid is the grid of elements used for the Berger et al. (1992) finite element hydrodynamic model of Galveston Bay.

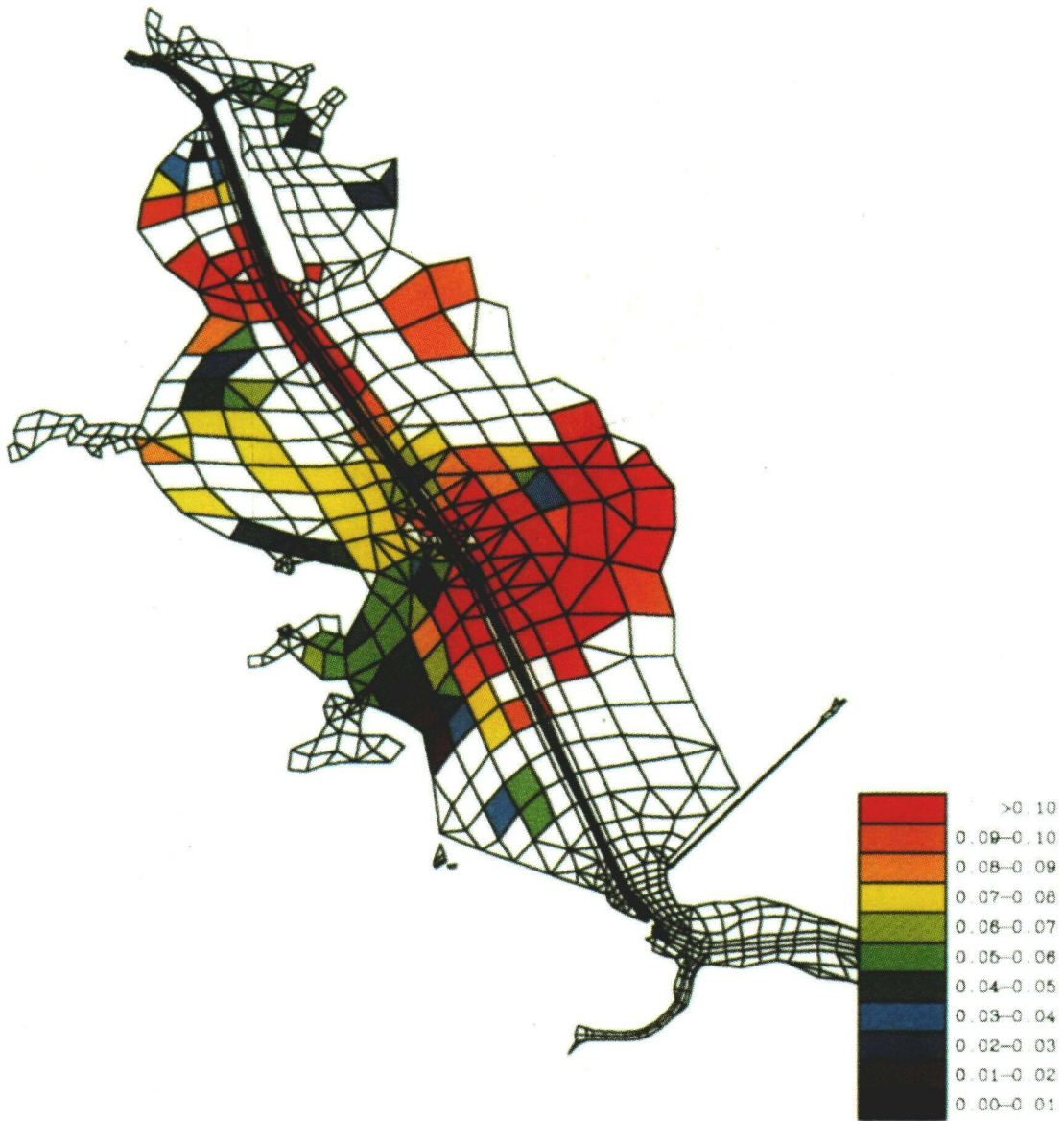
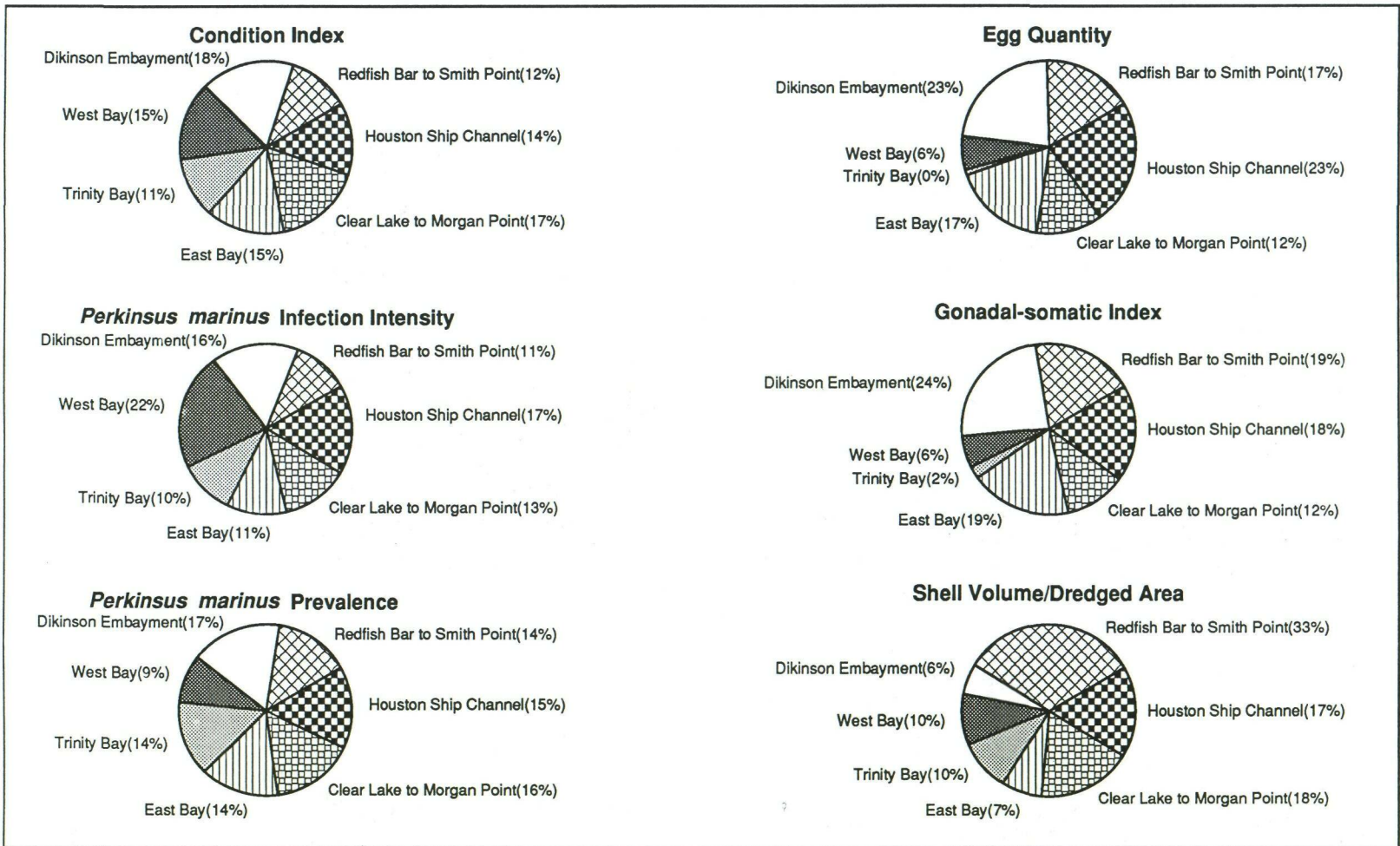
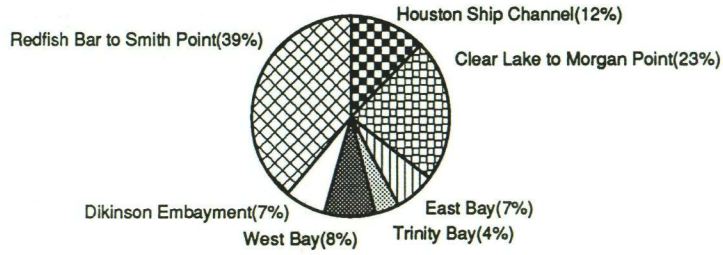


Figure 1 – Continued

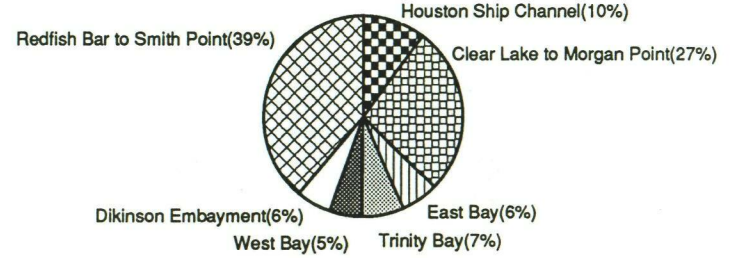
Figure 2. Comparison of variable means among bay sections, calculated for groups of sampling sites located in the seven sections of Galveston Bay defined in Table 1.



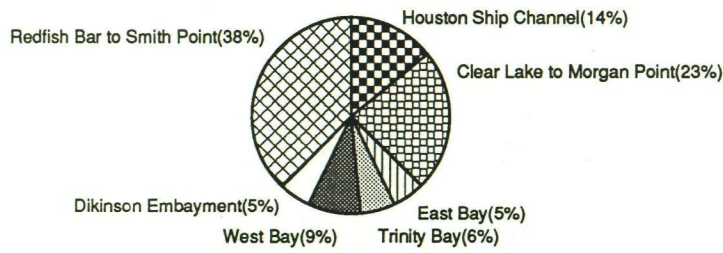
**Oyster Biomass**



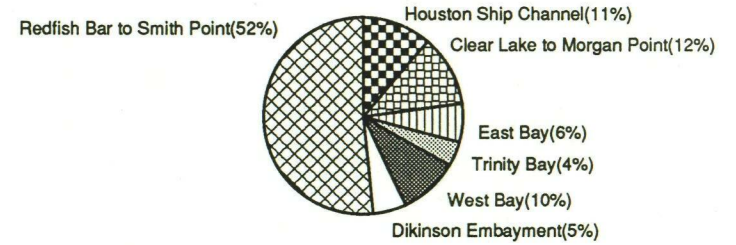
**Density of Submarket-sized Oysters**



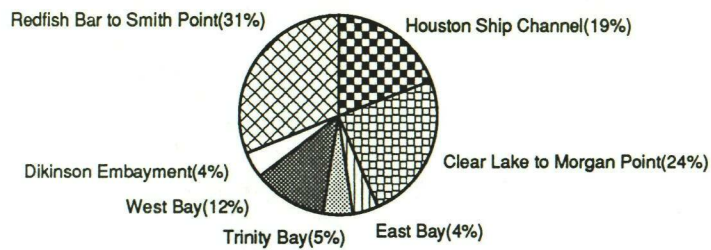
**Total Oyster Density**



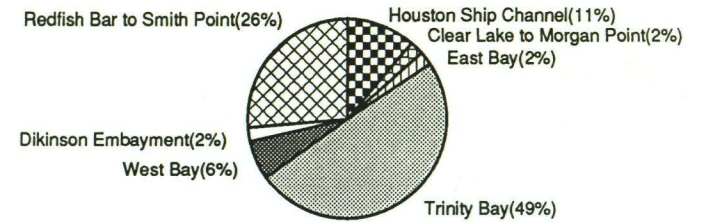
**Density of Market-sized Oysters**

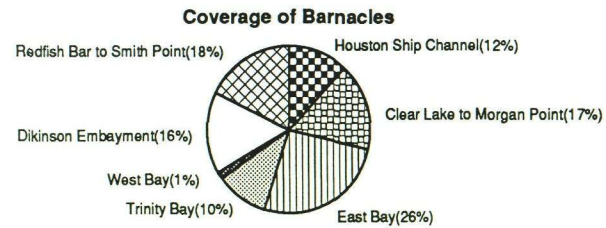
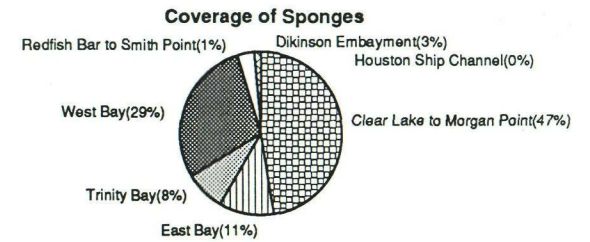
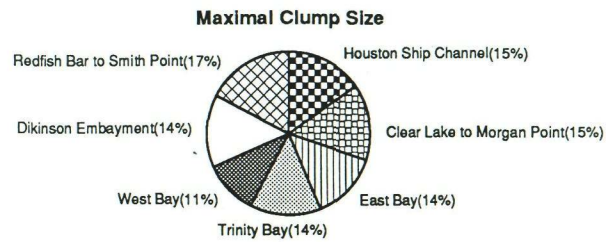
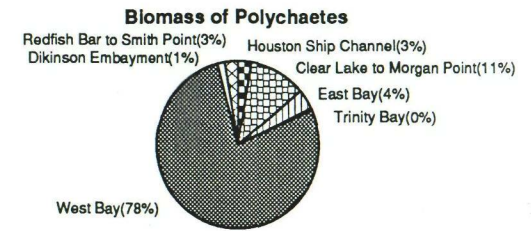
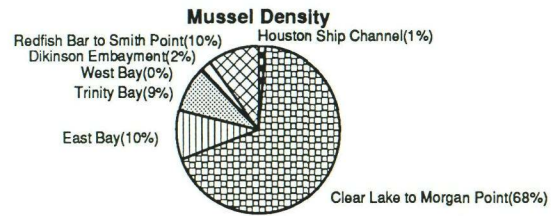
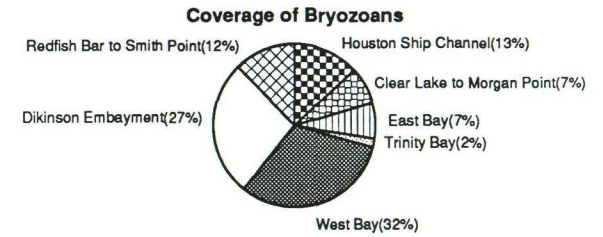
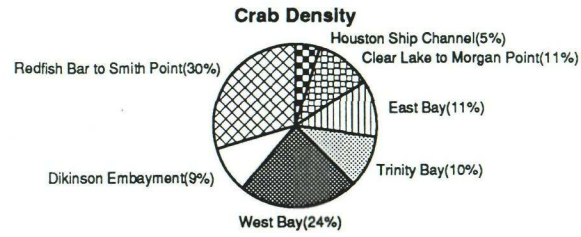


**Juvenile Oyster Density**



**Box Density**





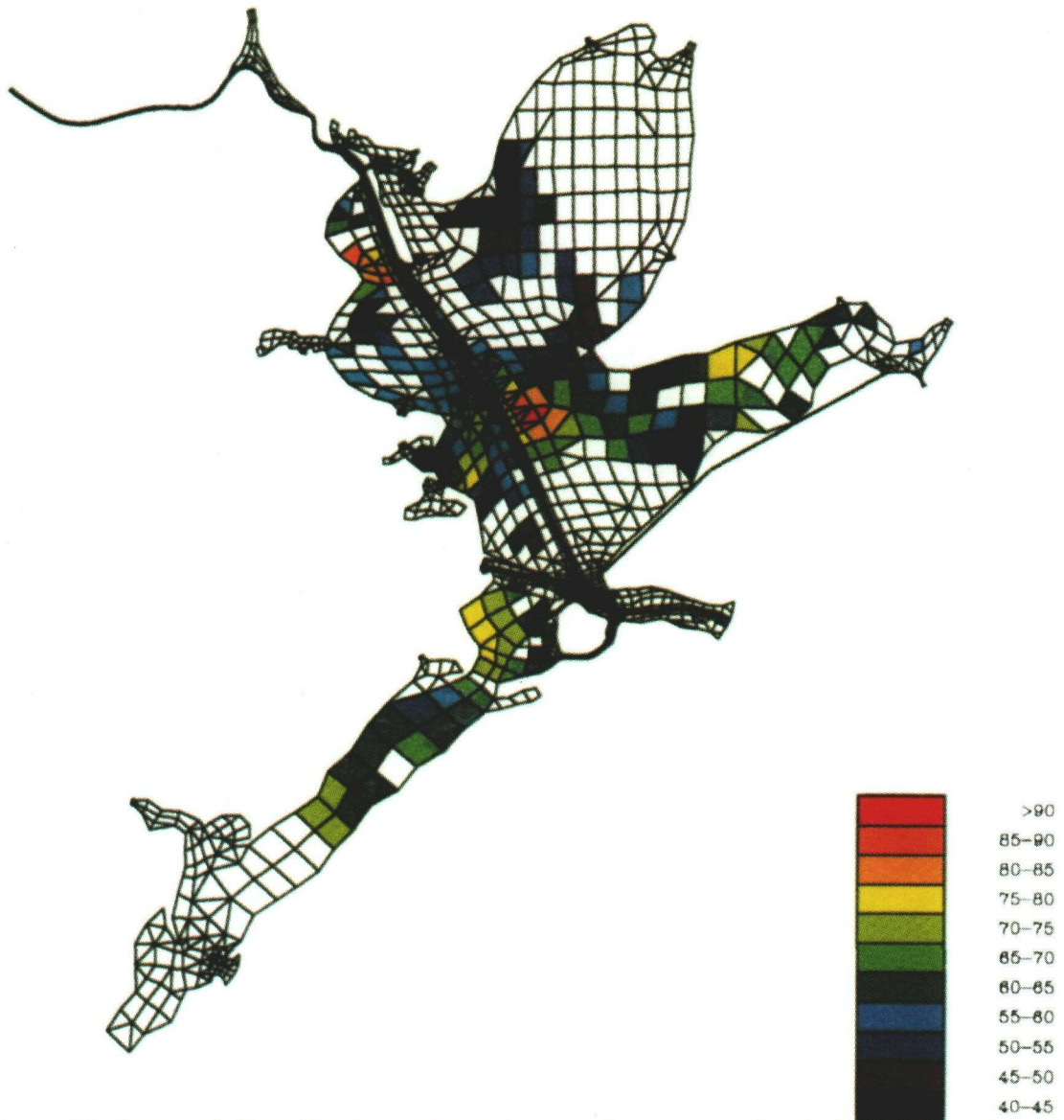


Figure 3. Estimated distribution of maximum clump size (cm) obtained using the 51 known sites to predict the values at all unsampled locations and a close-up of the estimated distribution of maximum clump size along the Houston Ship Channel. The grid is the grid of elements used for the Berger et al. (1992) finite element hydrodynamic model of Galveston Bay.

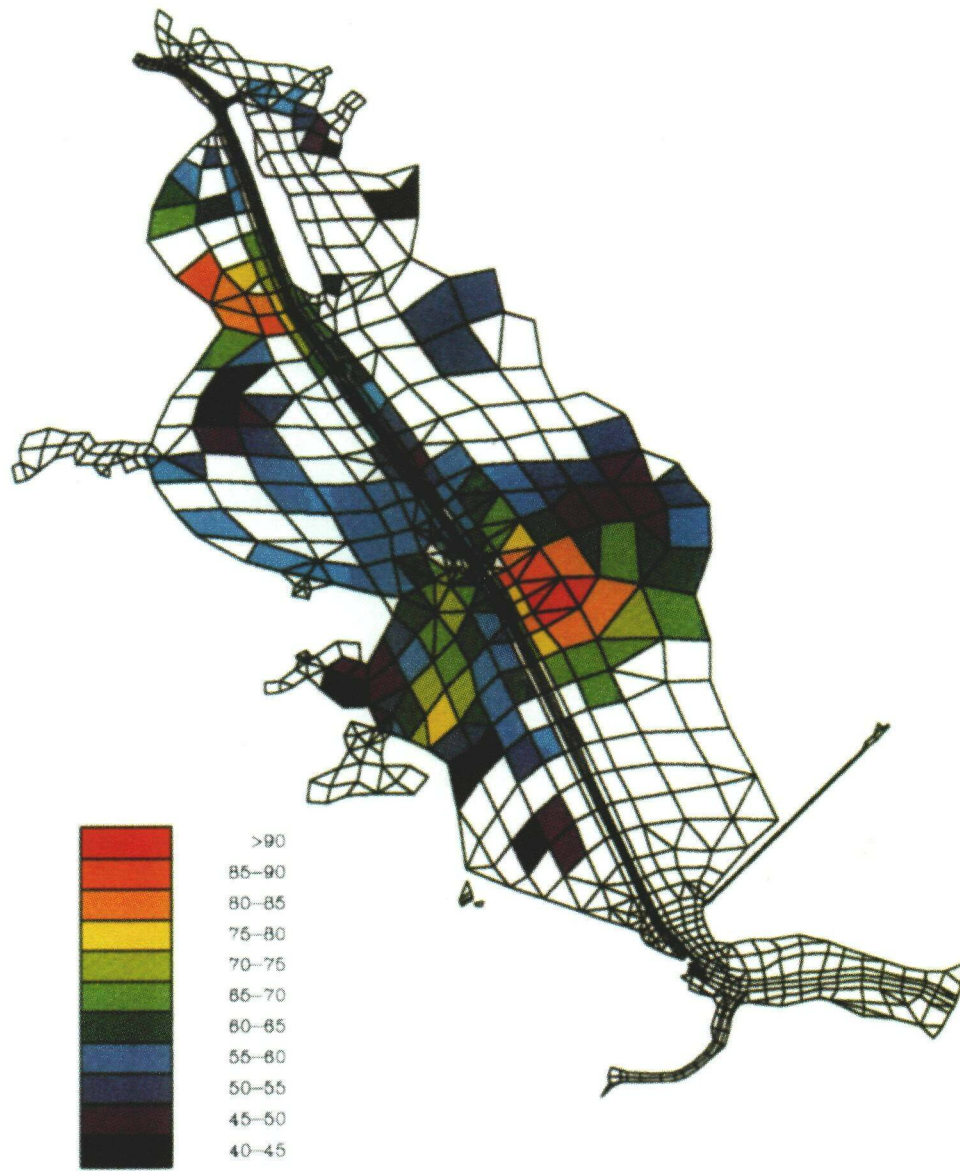


Figure 3 – Continued

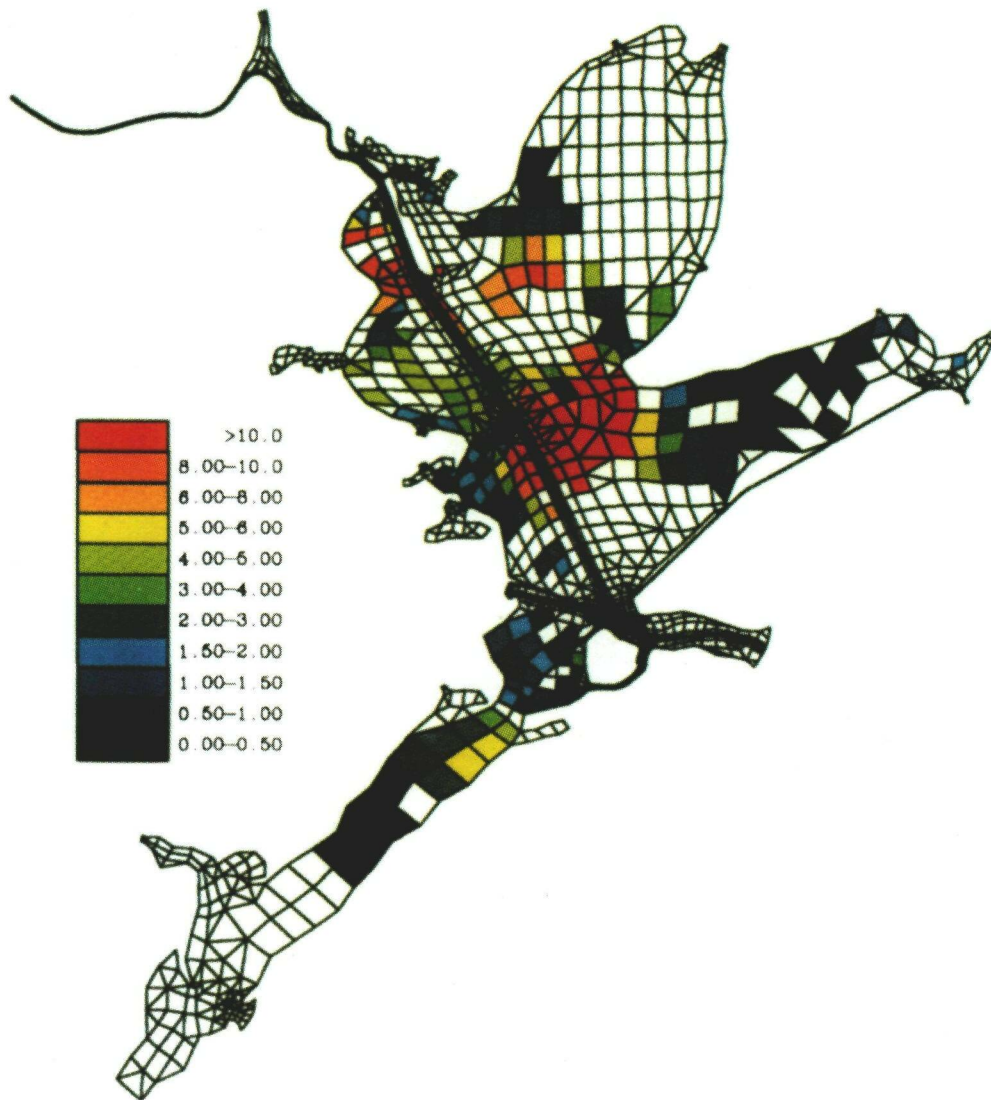


Figure 4. Estimated distribution of oysters (ind m<sup>-2</sup>) obtained using the 51 known sites to predict the values at all unsampled locations. The grid is the grid of elements used for the Berger et al. (1992) finite element hydrodynamic model of Galveston Bay.

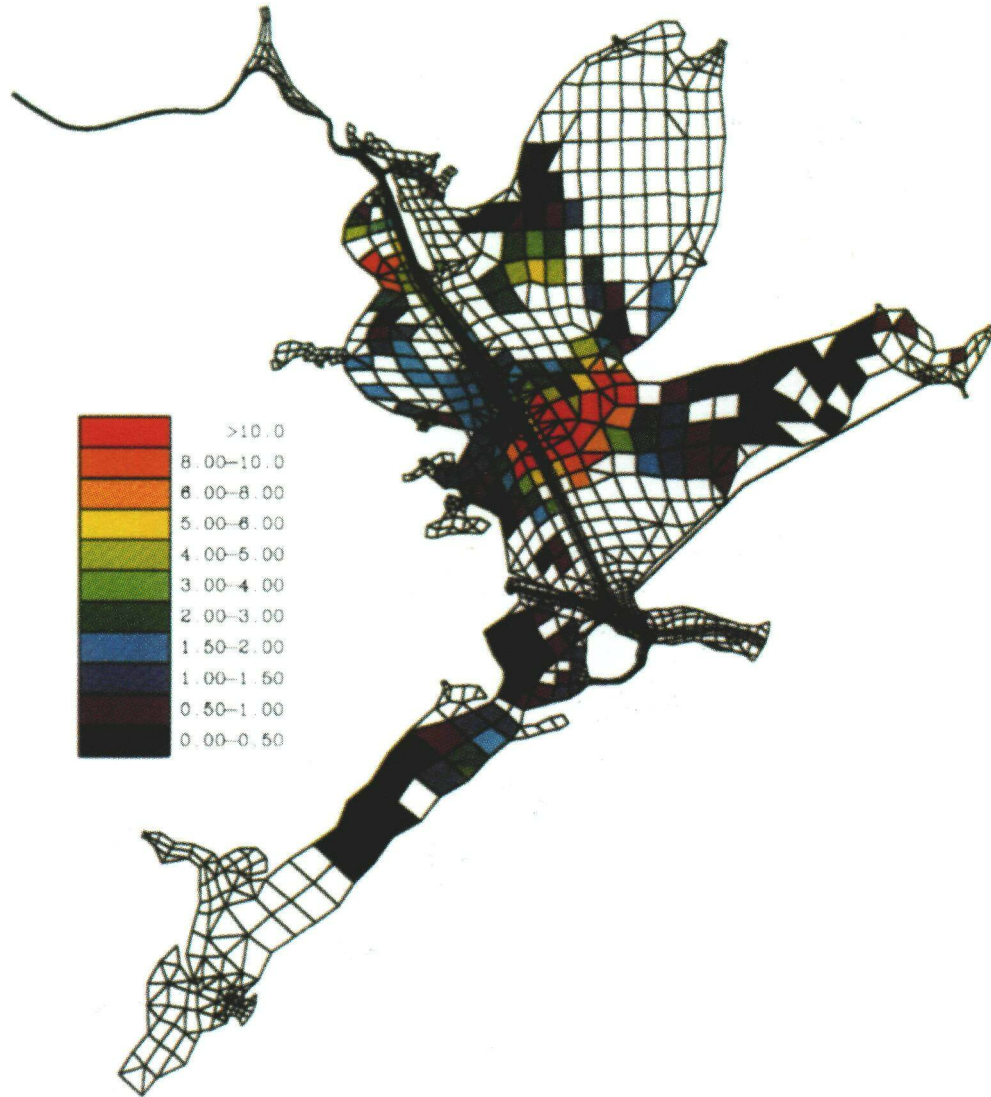


Figure 5. Estimated distribution of market-size oysters (ind m<sup>-2</sup>) obtained using the 51 known sites to predict the values at all unsampled locations and a close-up of the estimated distribution of adult oysters (ind m<sup>-2</sup>) along the Houston Ship Channel. The grid is the grid of elements used for the Berger et al. (1992) finite element hydrodynamic model of Galveston Bay.

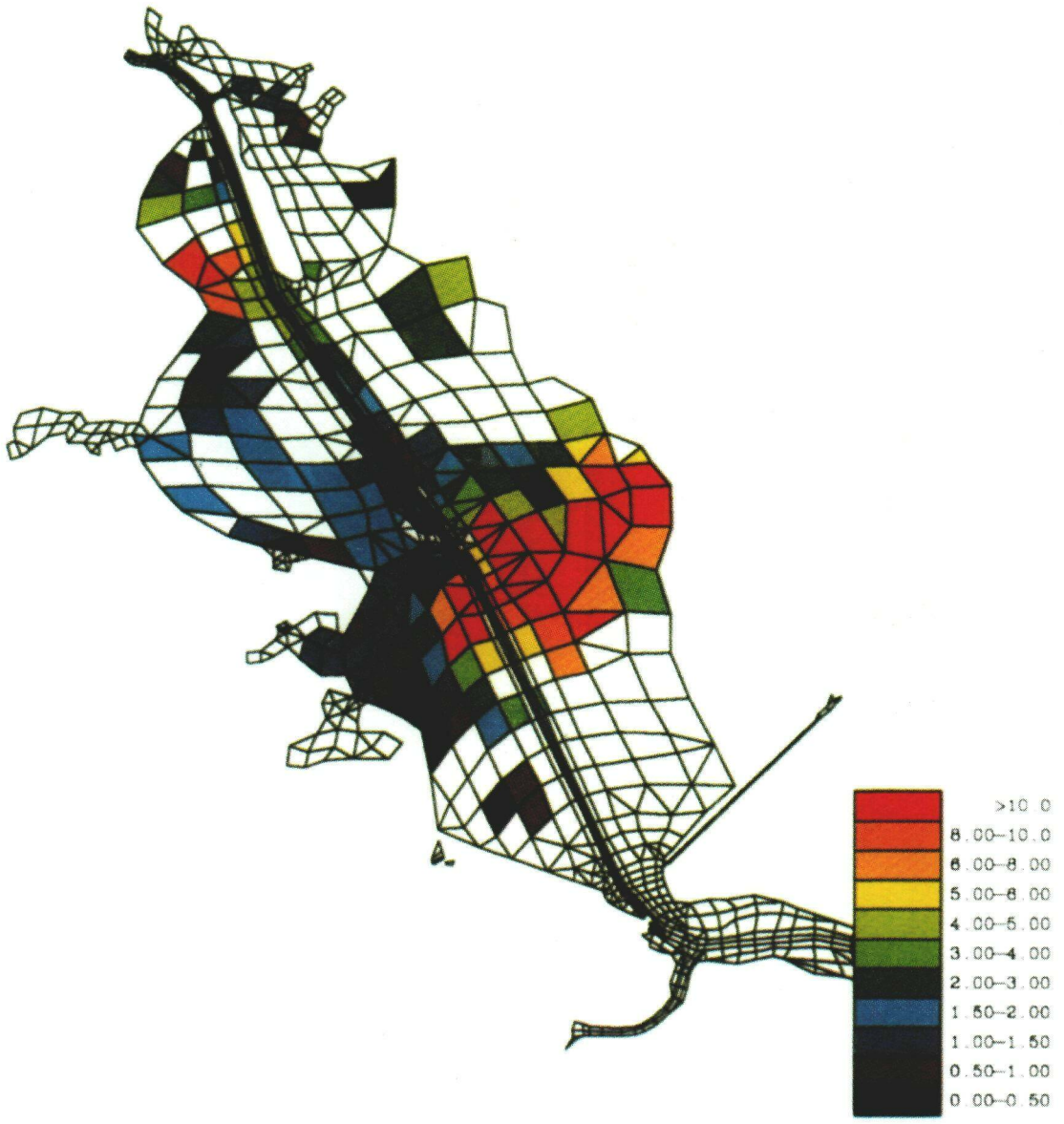


Figure 5 – Continued

Figure 6. Size-frequency distributions for oysters from the 51 sampled sites.

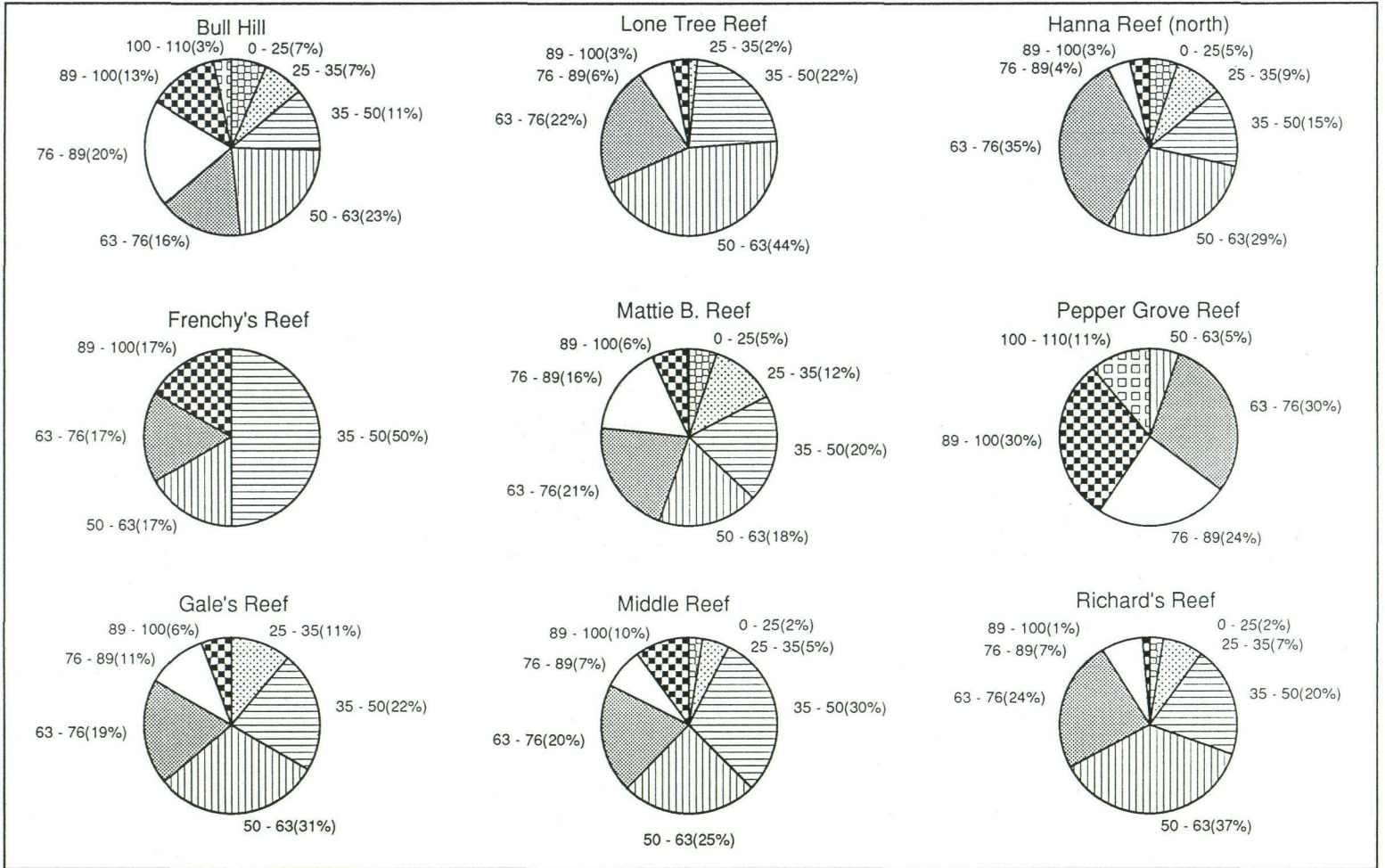


Figure 6—Continued

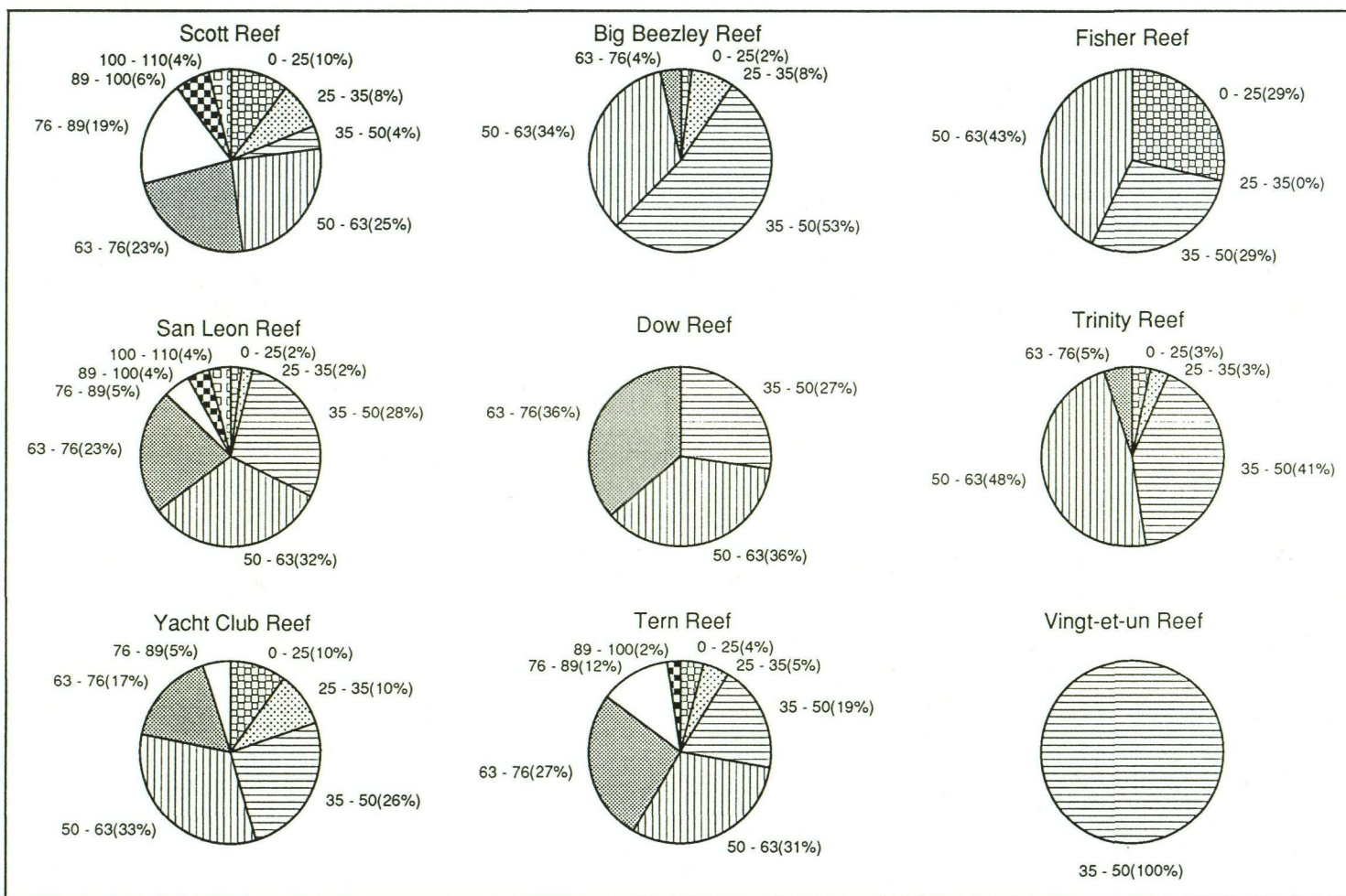


Figure 6 – Continued

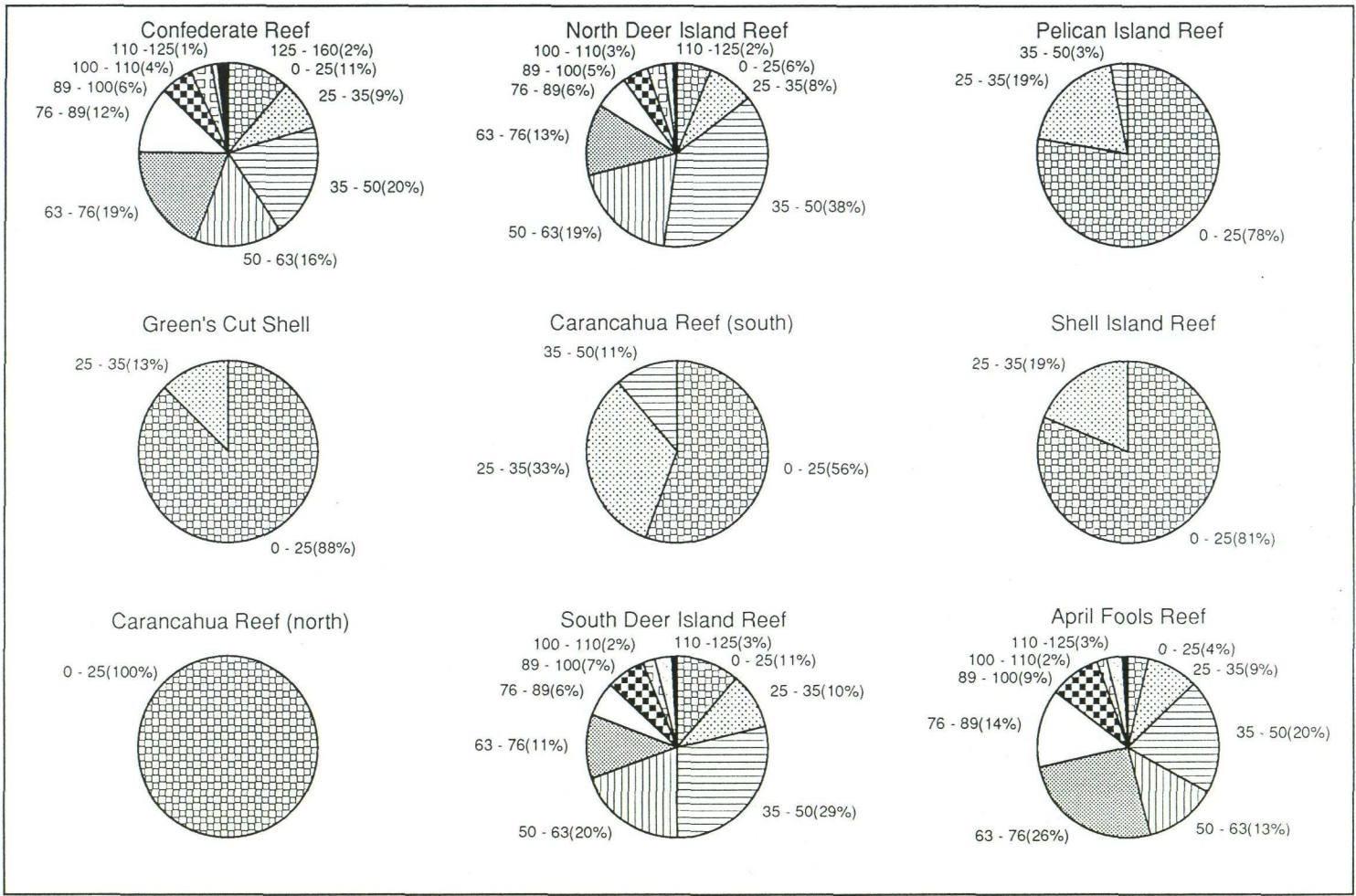
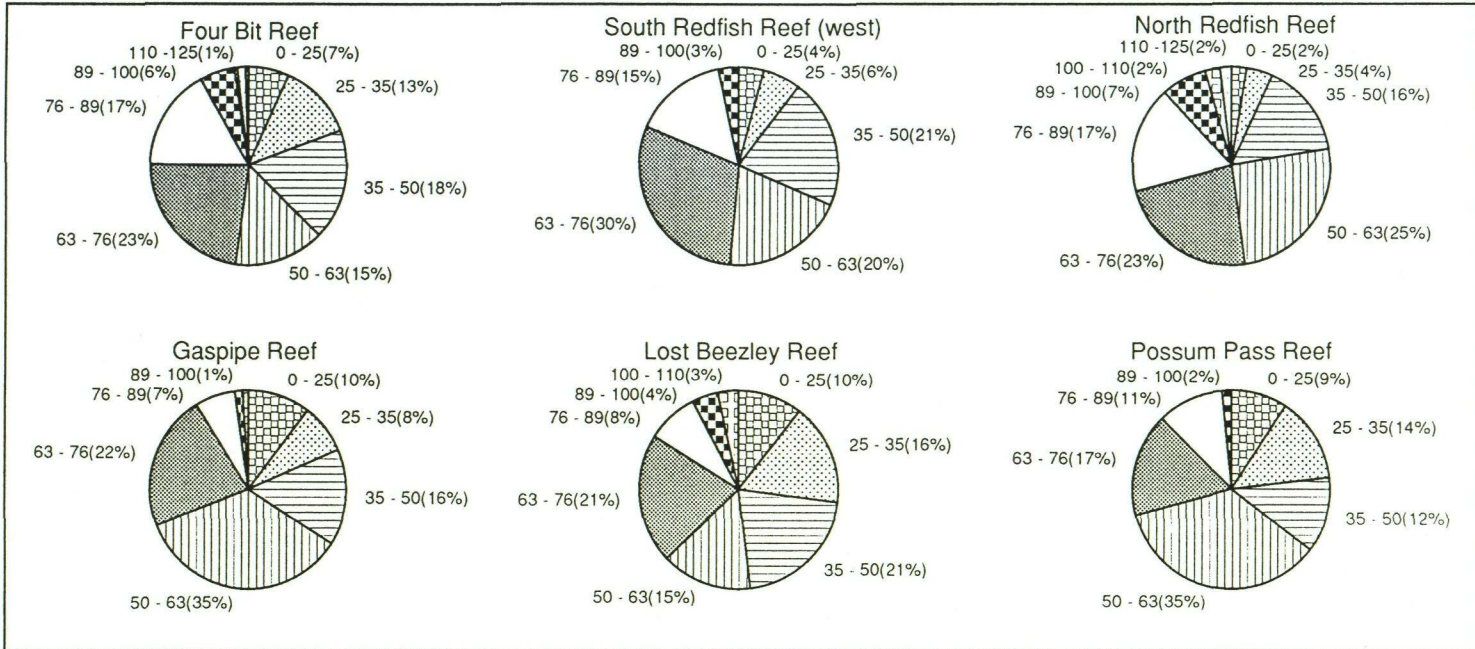


Figure 6 – Continued



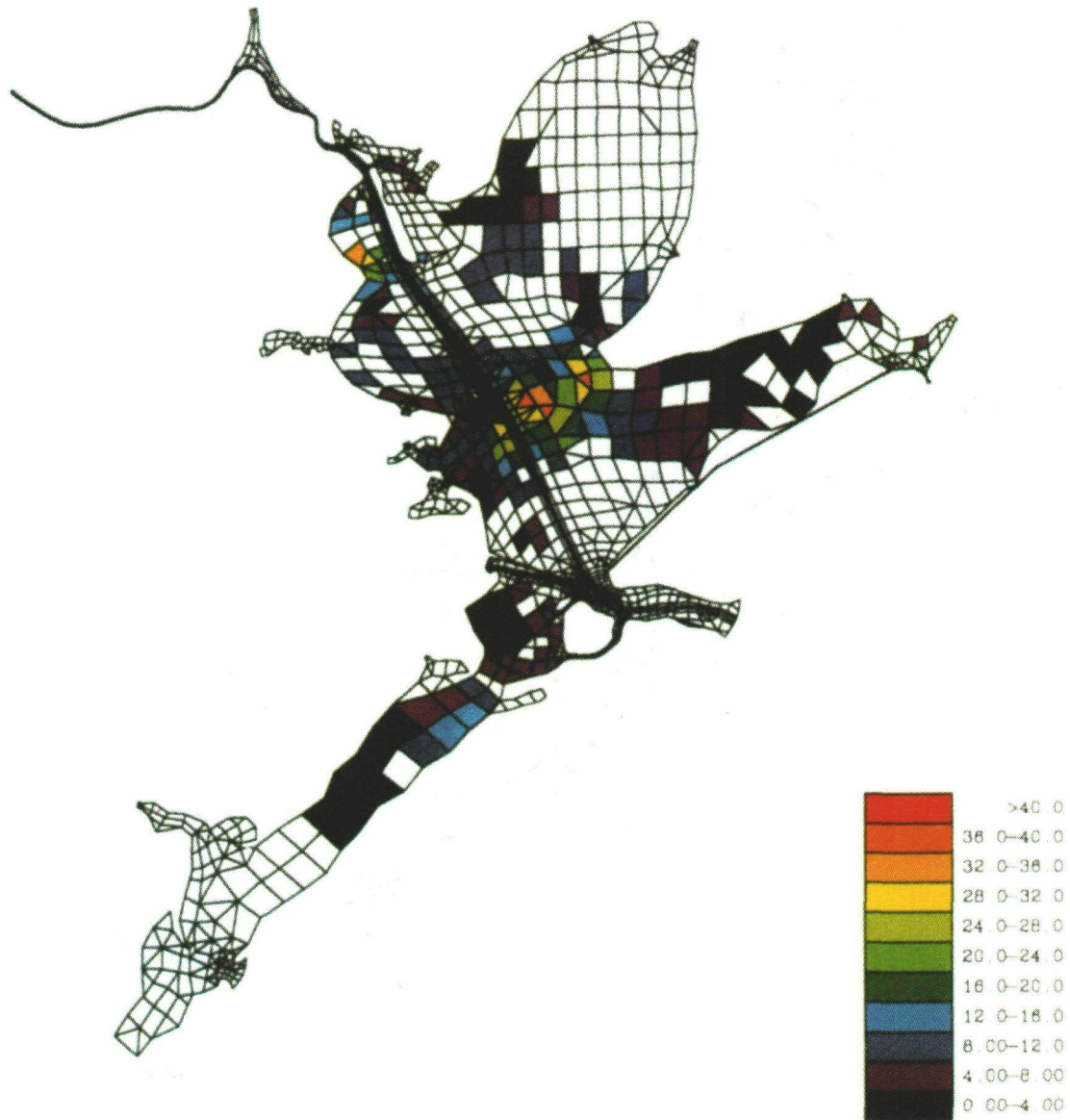


Figure 7. Estimated distribution of biomass (g dry wt m<sup>-2</sup>) obtained using the 51 known sites to predict the values at all unsampled locations and a close-up of the estimated distribution of biomass along the Houston Ship Channel. The grid is the grid of elements used for the Berger et al. (1992) finite element hydrodynamic model of Galveston Bay.

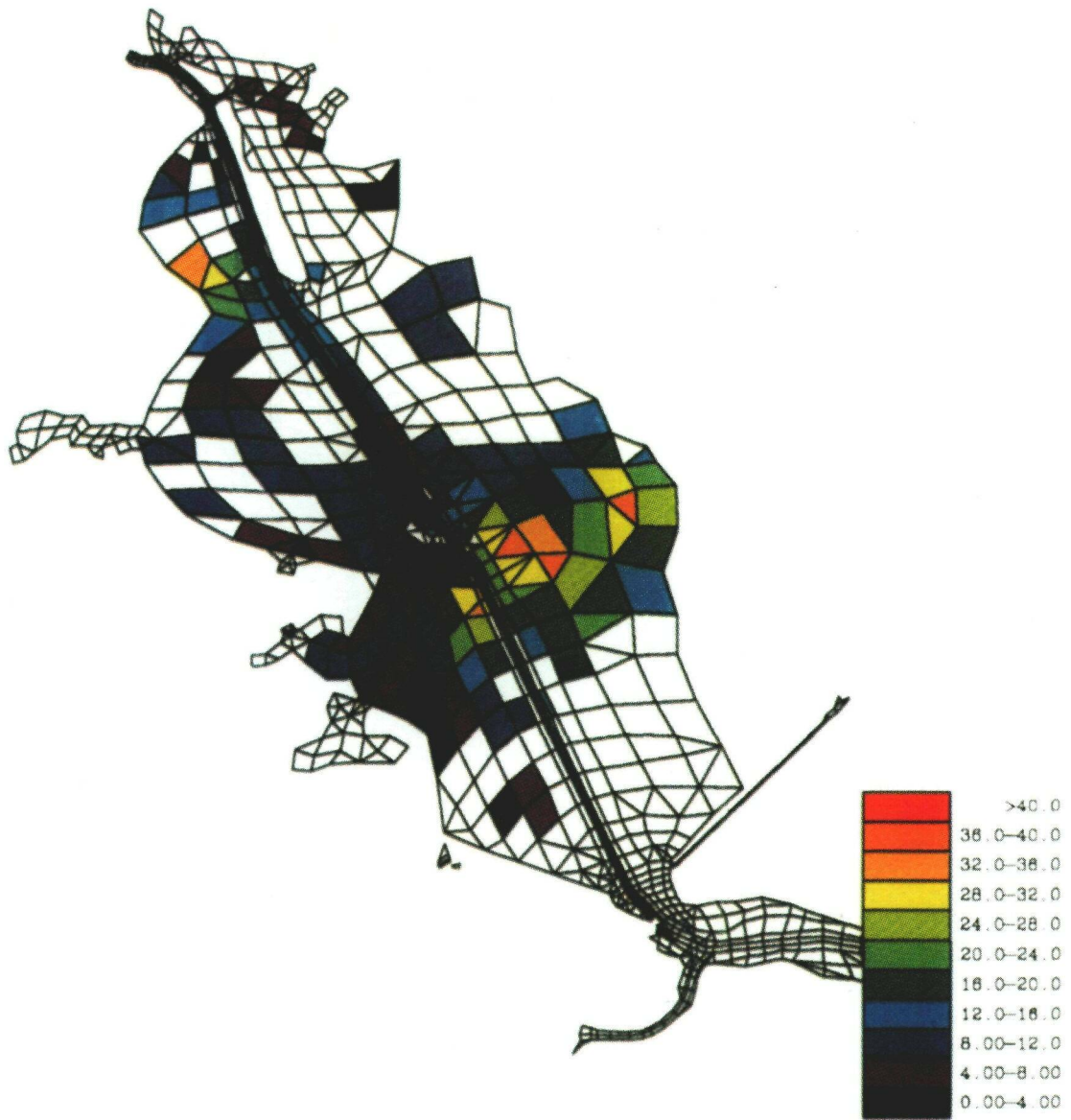


Figure 7 – Continued

### Correlations between oyster weight and shell length

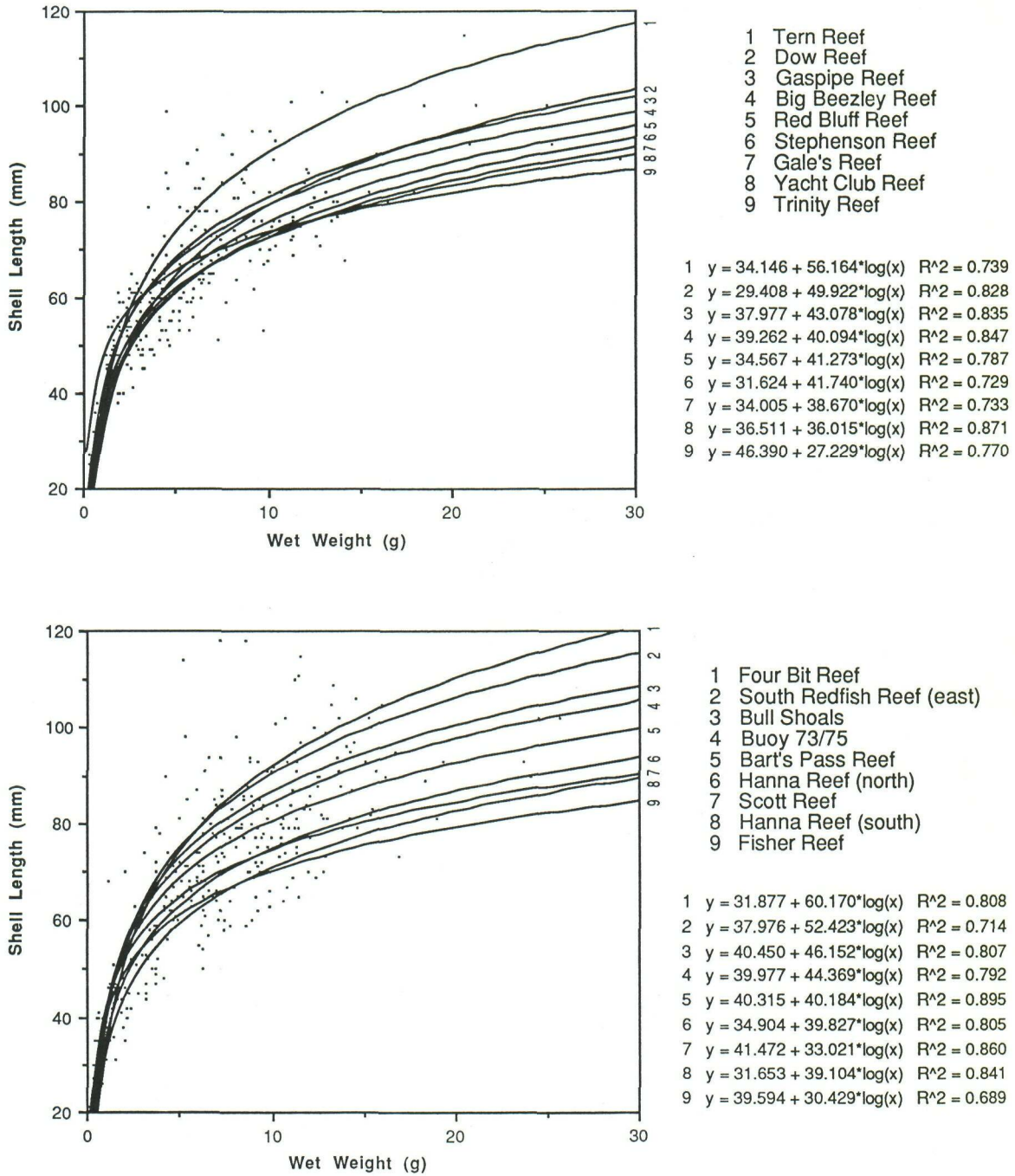
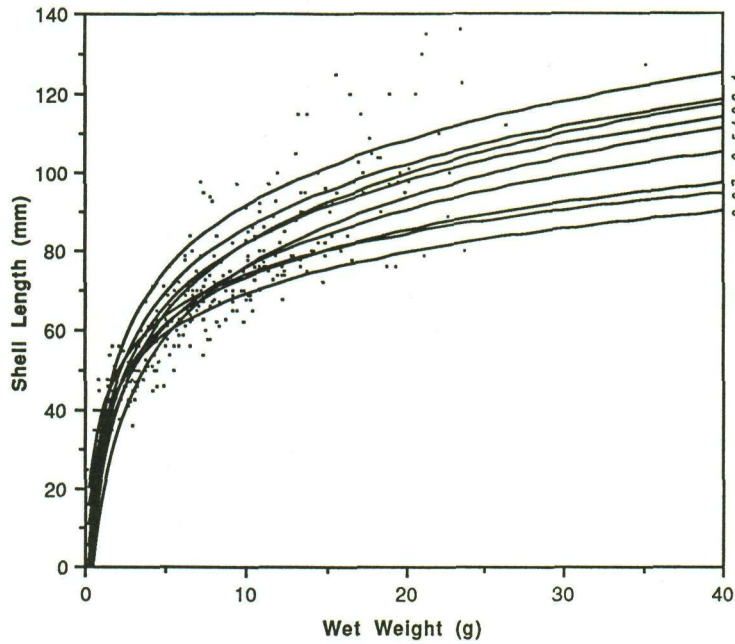
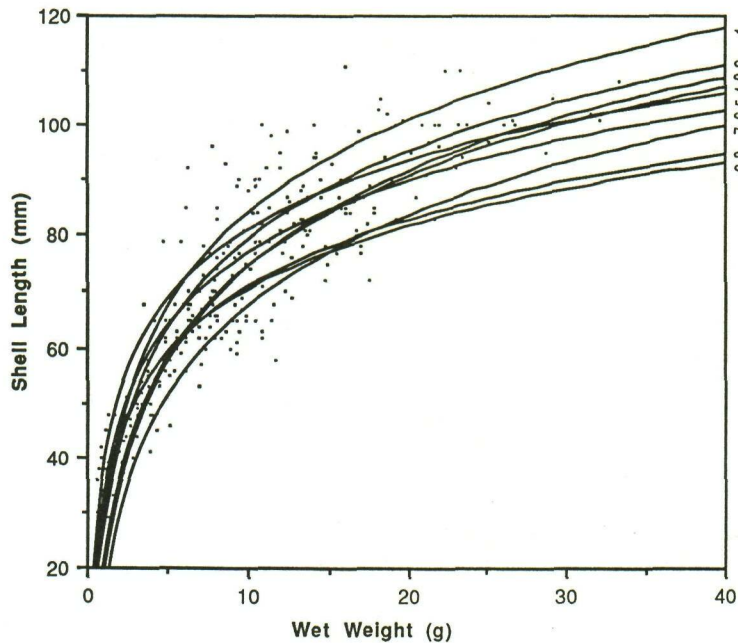


Figure 8. Length-biomass relationships for the 51 sampled sites. Best fit curves assume a semilog relationship between length and weight (Powell and Stanton, 1985).



- 1 South Deer Island Reef
- 2 North Deer Island Reef
- 3 April Fools Reef
- 4 Confederate Reef
- 5 Todd's Dump Reef
- 6 Dickinson Reef
- 7 Levee Reef
- 8 Morgan Point Reef
- 9 Half Moon Reef

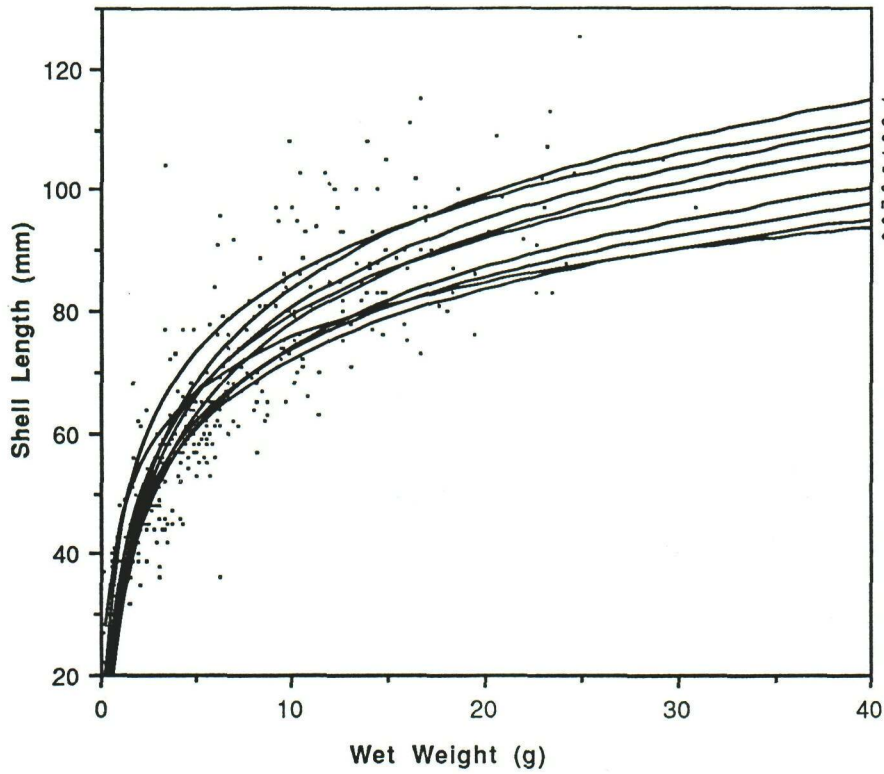
- 1  $y = 35.664 + 55.615 \cdot \log(x)$   $R^2 = 0.879$
- 2  $y = 31.106 + 54.379 \cdot \log(x)$   $R^2 = 0.795$
- 3  $y = 22.284 + 59.256 \cdot \log(x)$   $R^2 = 0.853$
- 4  $y = 28.399 + 53.299 \cdot \log(x)$   $R^2 = 0.740$
- 5  $y = 16.495 + 59.049 \cdot \log(x)$   $R^2 = 0.586$
- 6  $y = 26.288 + 49.167 \cdot \log(x)$   $R^2 = 0.812$
- 7  $y = 33.025 + 39.994 \cdot \log(x)$   $R^2 = 0.847$
- 8  $y = 39.192 + 34.556 \cdot \log(x)$   $R^2 = 0.817$
- 9  $y = 34.533 + 34.452 \cdot \log(x)$   $R^2 = 0.871$



- 1 Mattie B. Reef
- 2 Buoy 59
- 3 Pepper Grove Reef
- 4 San Leon Reef
- 5 South Redfish Reef (west)
- 6 Bull Hill
- 7 Frenchy's Reef
- 8 Whitehead Reef
- 9 Dollar Reef

- 1  $y = 28.111 + 55.882 \cdot \log(x)$   $R^2 = 0.873$
- 2  $y = 26.419 + 52.746 \cdot \log(x)$   $R^2 = 0.869$
- 3  $y = 17.319 + 56.983 \cdot \log(x)$   $R^2 = 0.739$
- 4  $y = 20.528 + 53.881 \cdot \log(x)$   $R^2 = 0.885$
- 5  $y = 39.698 + 41.211 \cdot \log(x)$   $R^2 = 0.853$
- 6  $y = 33.890 + 42.902 \cdot \log(x)$   $R^2 = 0.896$
- 7  $y = 13.626 + 53.718 \cdot \log(x)$   $R^2 = 0.917$
- 8  $y = 31.608 + 39.271 \cdot \log(x)$   $R^2 = 0.834$
- 9  $y = 32.751 + 37.566 \cdot \log(x)$   $R^2 = 0.817$

Figure 8 – Continued



- 1 Buoy 63
- 2 Lost Beezley Reef
- 3 East Redfish Reef
- 4 North Redfish Reef
- 5 Richard's Reef
- 6 Buoy 53/55
- 7 Middle Reef
- 8 Lone Tree Reef
- 9 Possum Pass Reef

- 1  $y = 31.923 + 51.579 \cdot \log(x)$   $R^2 = 0.790$
- 2  $y = 43.492 + 42.115 \cdot \log(x)$   $R^2 = 0.809$
- 3  $y = 31.387 + 48.876 \cdot \log(x)$   $R^2 = 0.797$
- 4  $y = 28.355 + 49.244 \cdot \log(x)$   $R^2 = 0.767$
- 5  $y = 36.479 + 42.607 \cdot \log(x)$   $R^2 = 0.789$
- 6  $y = 29.995 + 43.836 \cdot \log(x)$   $R^2 = 0.731$
- 7  $y = 33.807 + 39.683 \cdot \log(x)$   $R^2 = 0.851$
- 8  $y = 33.230 + 38.579 \cdot \log(x)$   $R^2 = 0.839$
- 9  $y = 44.941 + 30.511 \cdot \log(x)$   $R^2 = 0.803$

Figure 8 – Continued

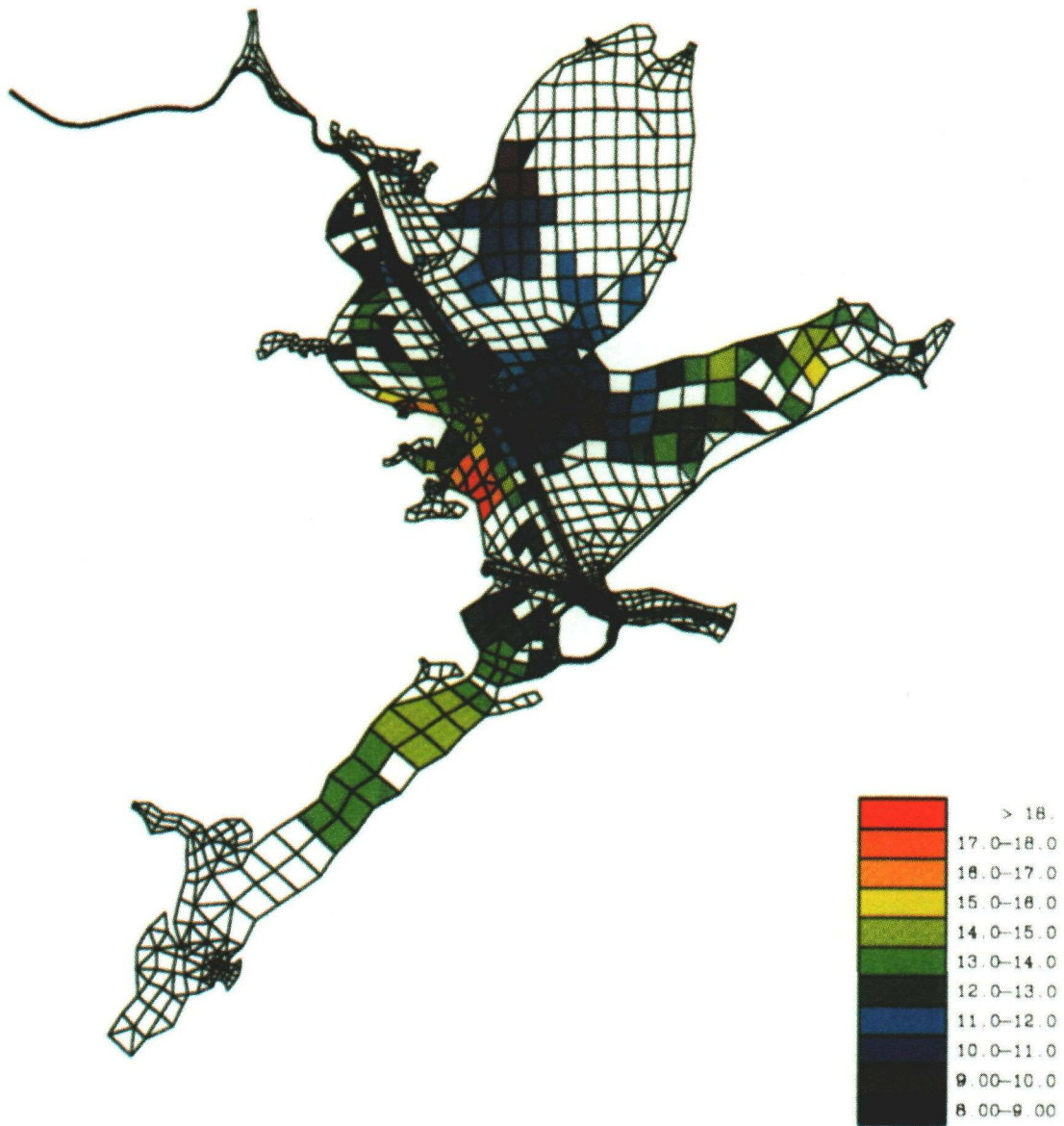


Figure 9. Estimated distribution of condition index in market-size adults (g dry wt ml<sup>-1</sup> \* 100) obtained using the 51 known sites to predict the values at all unsampled locations. The grid is the grid of elements used for the Berger et al. (1992) finite element hydrodynamic model of Galveston Bay.

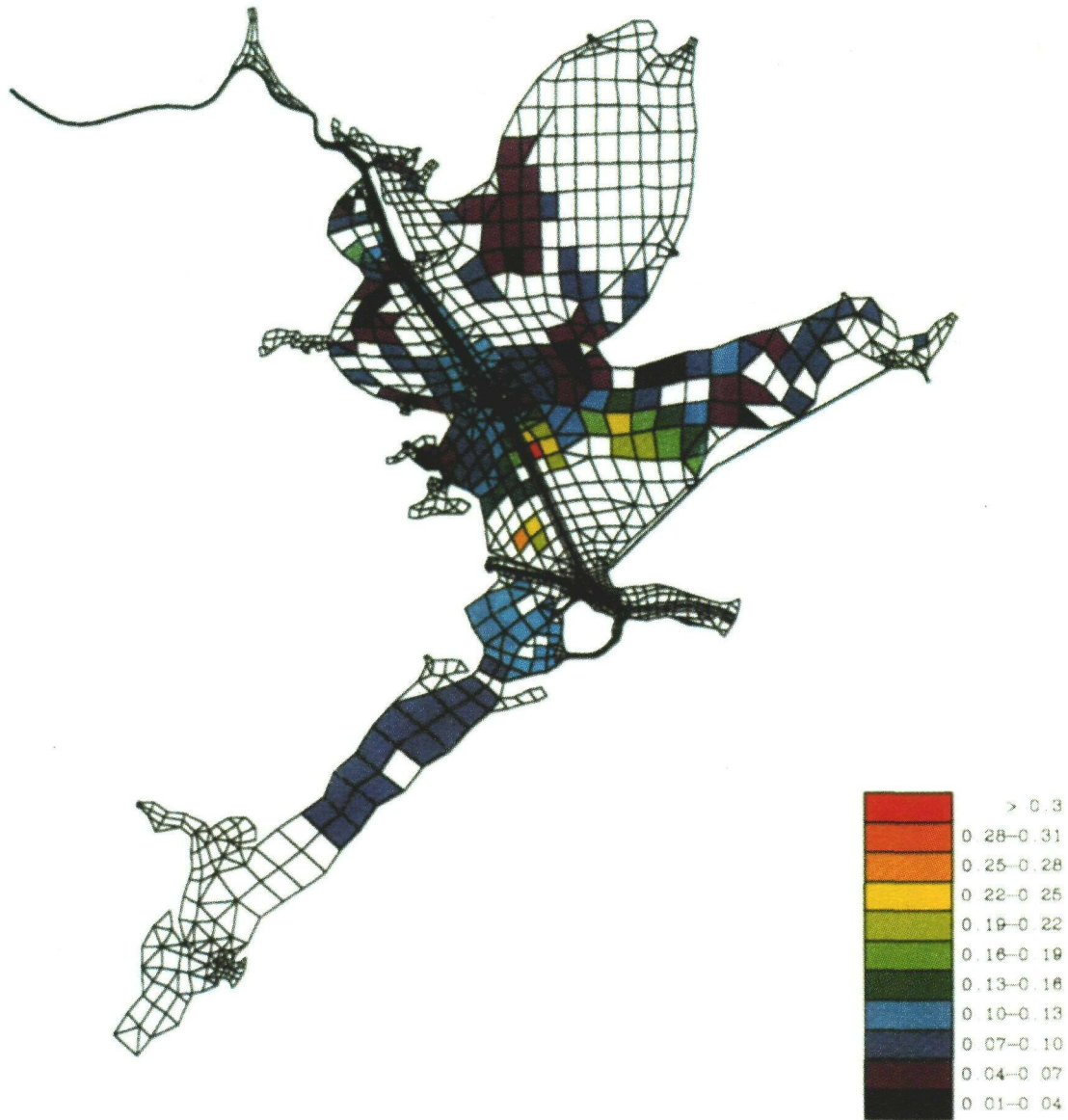


Figure 10. Estimated distribution of gonadal-somatic index in adult oysters (g dry wt egg g dry wt somatic tissue<sup>-1</sup>) obtained using the 51 known sites to predict the values at all unsampled locations. The grid is the grid of elements used for the Berger et al. (1992) finite element hydrodynamic model of Galveston Bay.

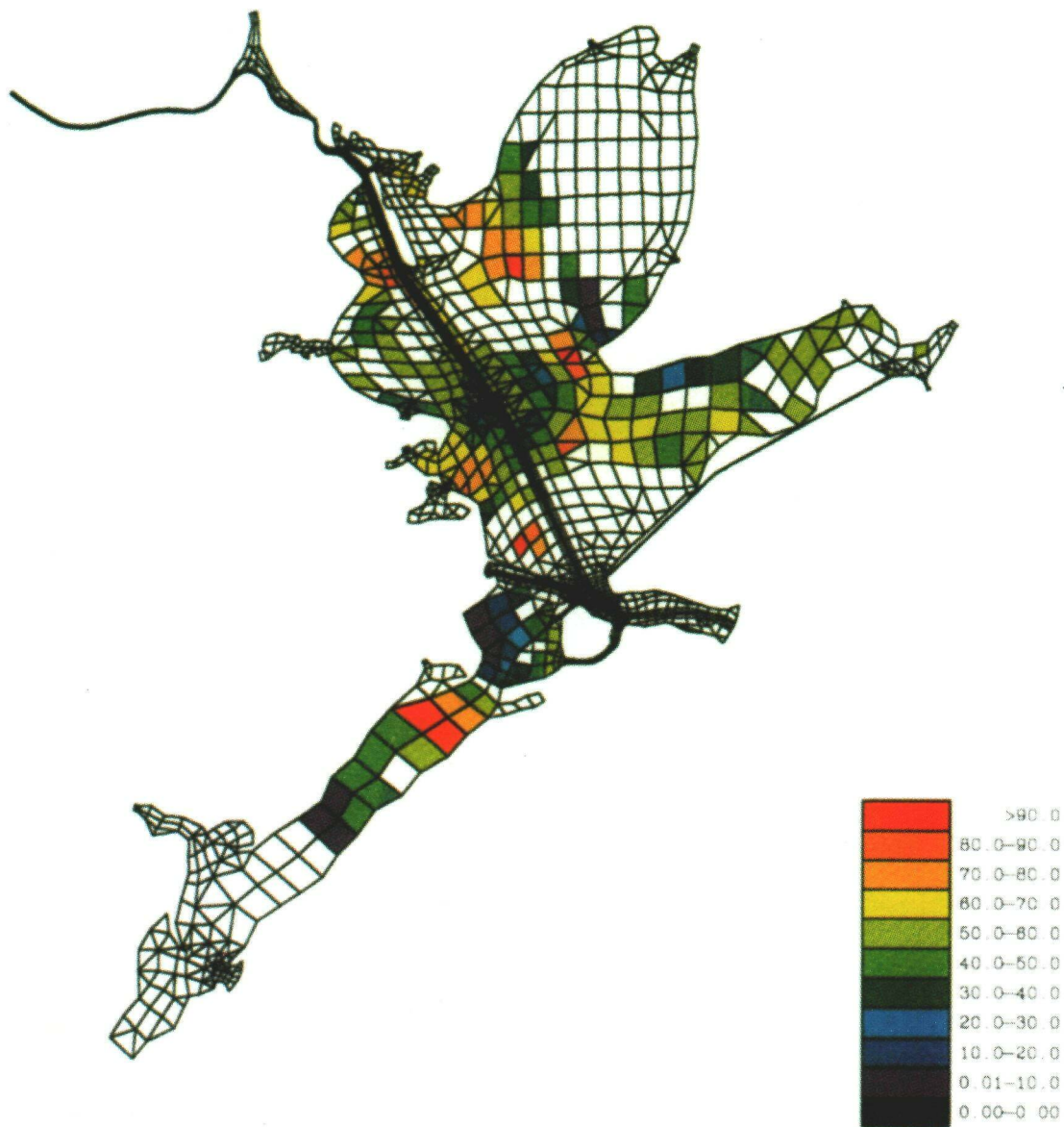


Figure 11. Estimated distribution prevalence of *P. marinus* obtained using the 51 known sites to predict the values at all unsampled locations and a close-up of the estimated distribution of *P. marinus* prevalence along the Houston Ship Channel. The grid is the grid of elements used for the Berger et al. (1992) finite element hydrodynamic model of Galveston Bay.

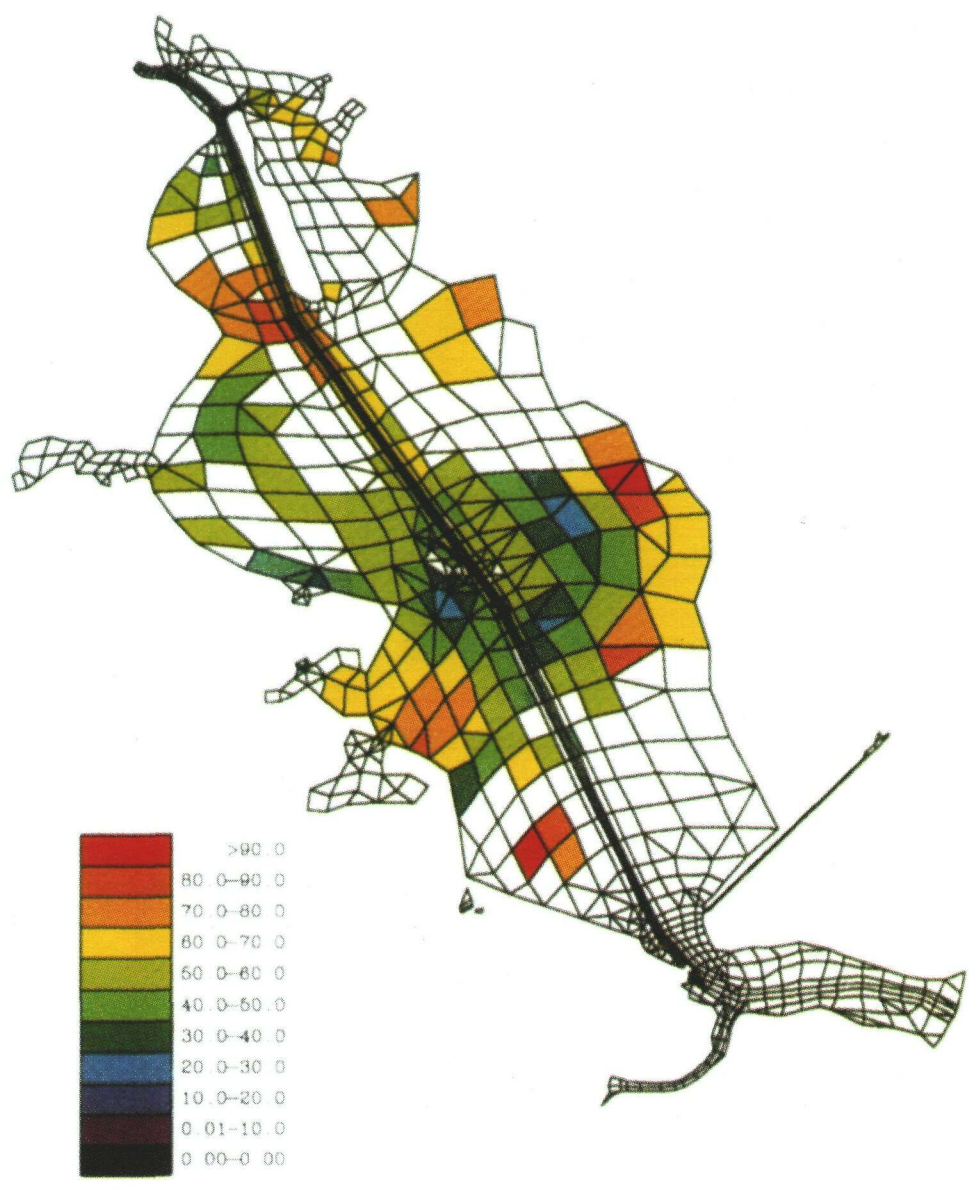


Figure 11 – Continued

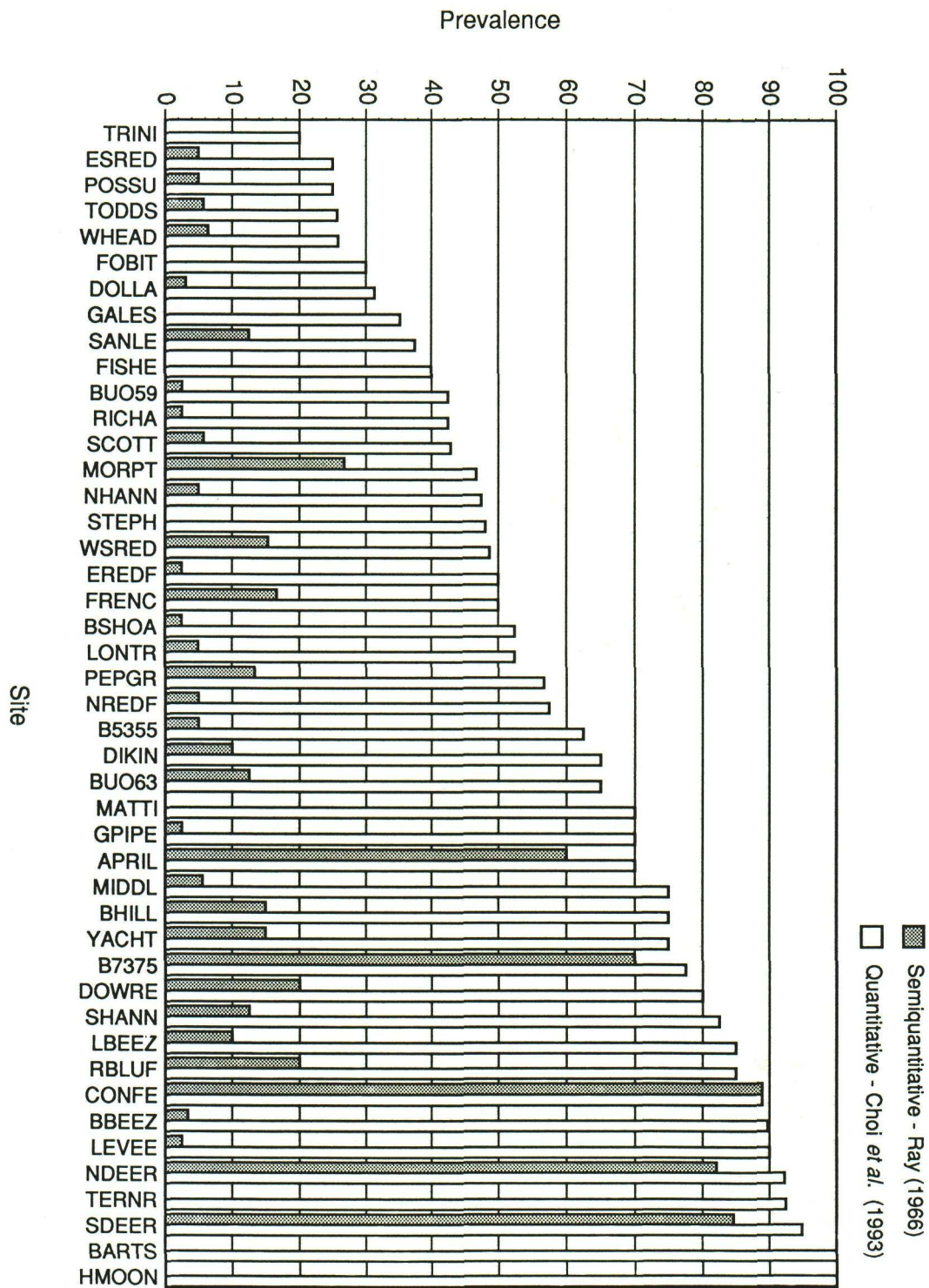


Figure 12. Comparison of *P. marinus* prevalence using the semiquantitative method of Ray (1966) and the quantitative method of Wilson et al. (in press).

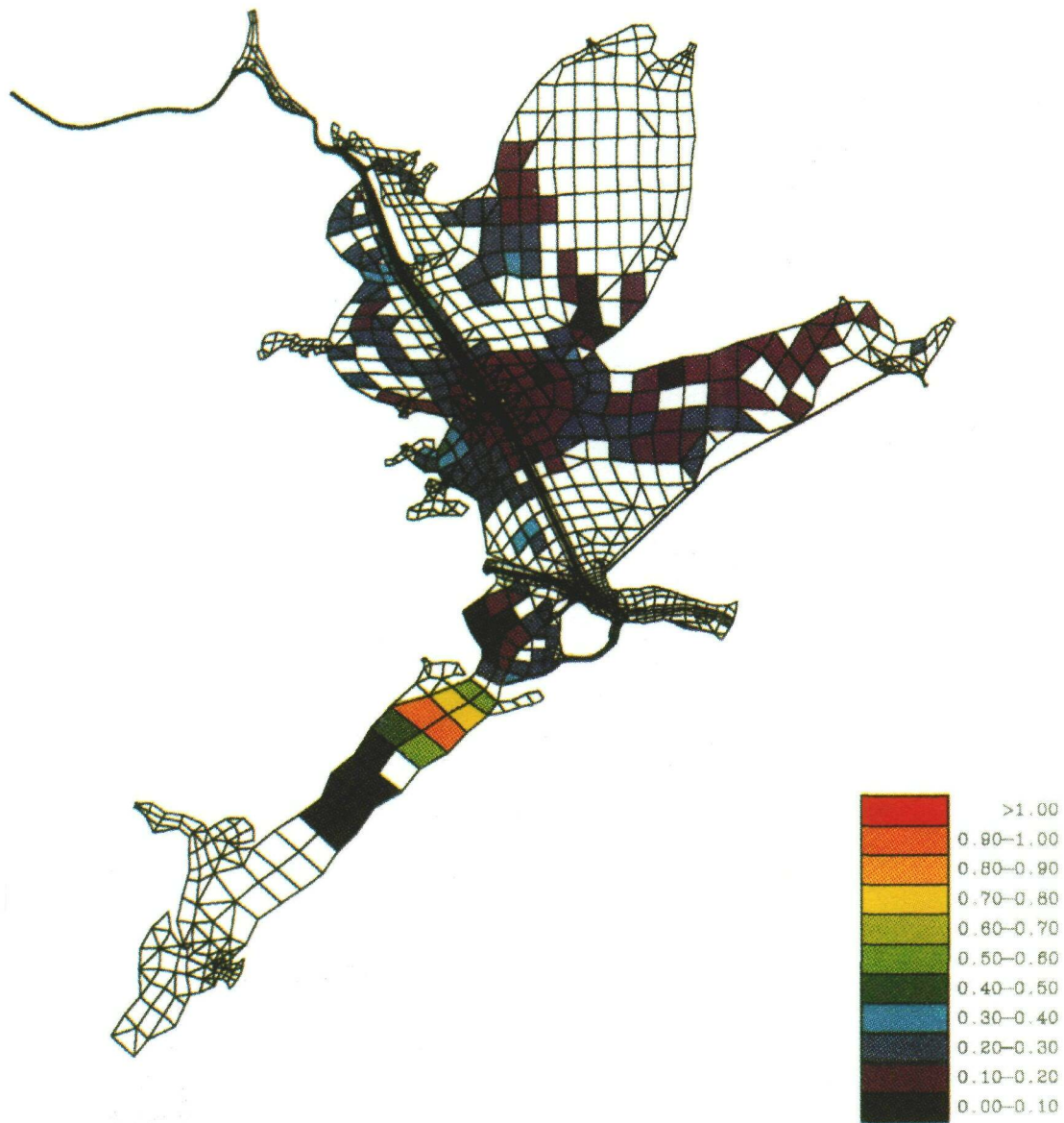


Figure 13. Estimated distribution infection intensity of *P. marinus* (Mackin's units) obtained using the 51 known sites to predict the values at all unsampled locations and a close-up of the estimated distribution of *P. marinus* infection intensity along the Houston Ship Channel. The grid is the grid of elements used for the Berger et al. (1992) finite element hydrodynamic model of Galveston Bay.

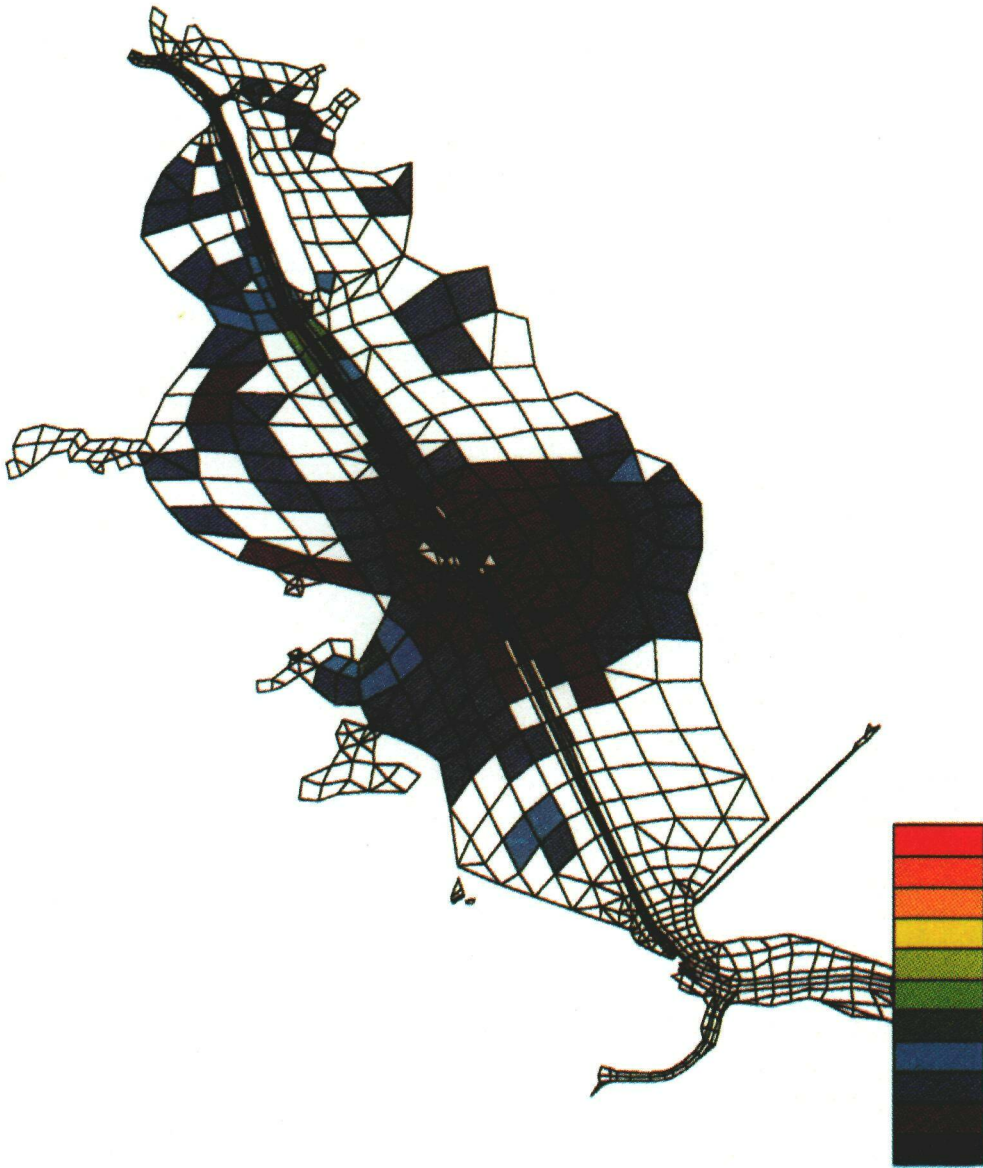


Figure 13 – Continued

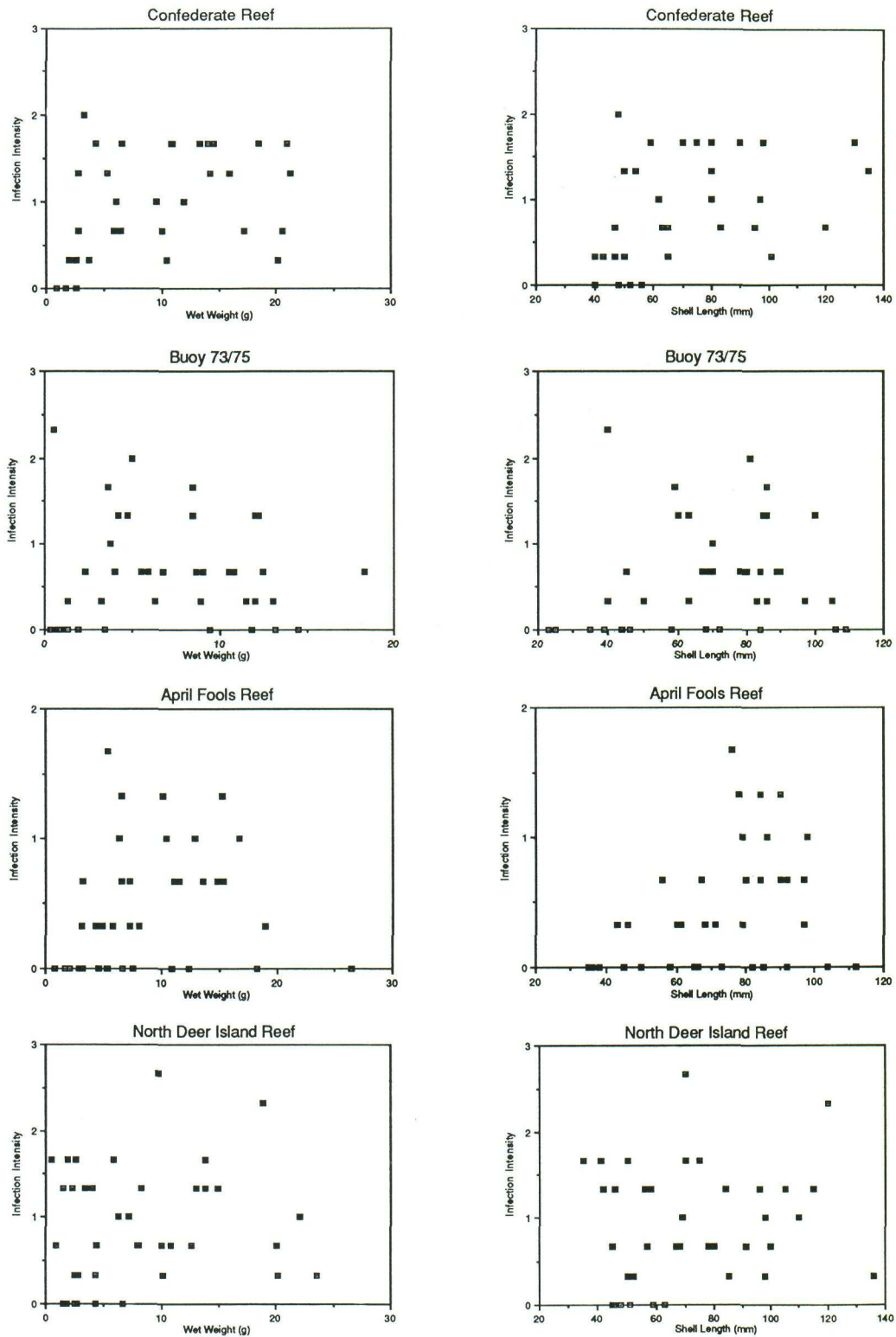


Figure 14. Example plots of *P. marinus* infection intensity versus anterior-posterior length or biomass (g wet meat wt) chosen as typical for broad areas of Galveston Bay.

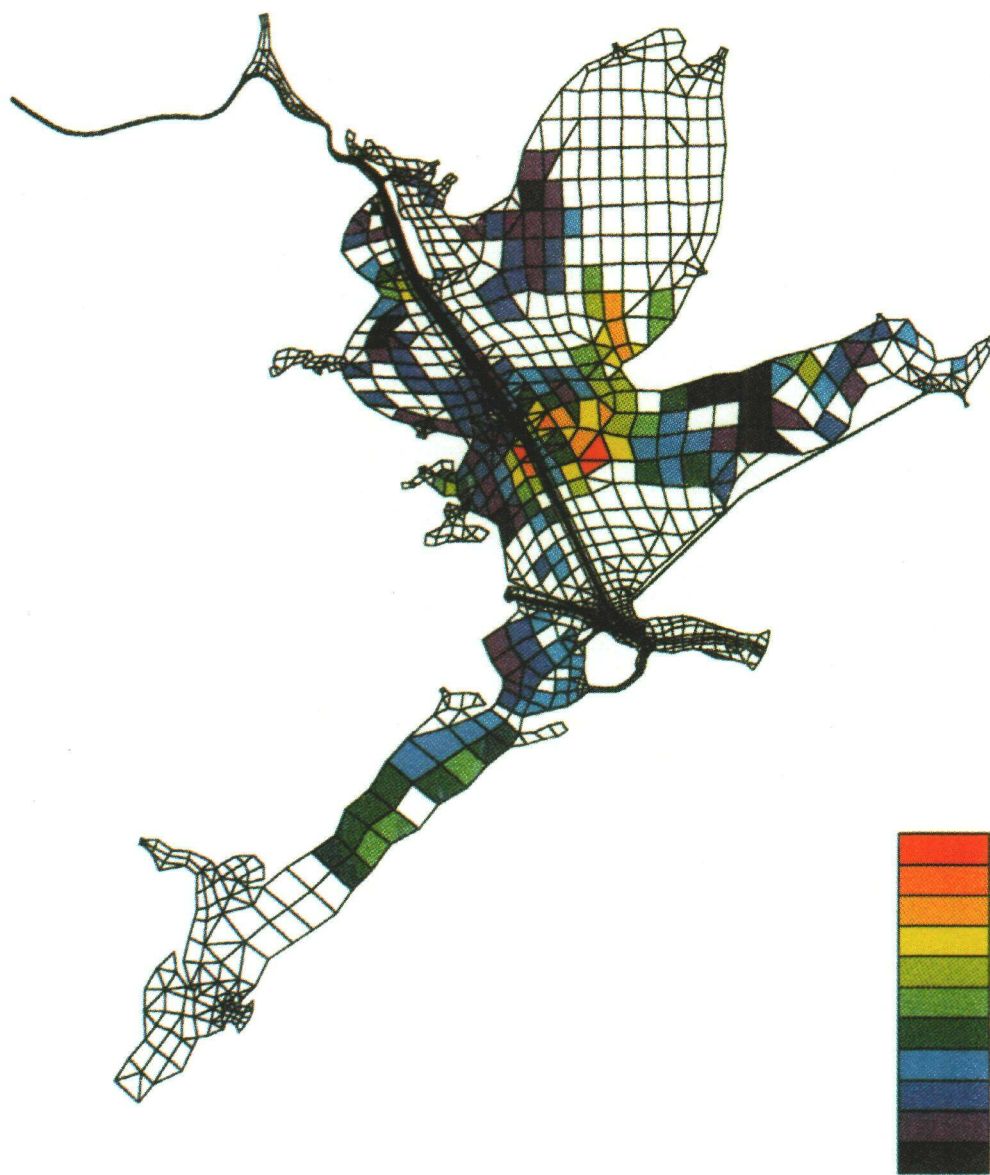


Figure 15. Estimated distribution of crabs ( $\text{ind m}^{-2}$ ) obtained using the 51 known sites to predict the values at all unsampled locations and a close-up of the estimated distribution of crabs along the Houston Ship Channel. The grid is the grid of elements used for the Berger et al. (1992) finite element hydrodynamic model of Galveston Bay.

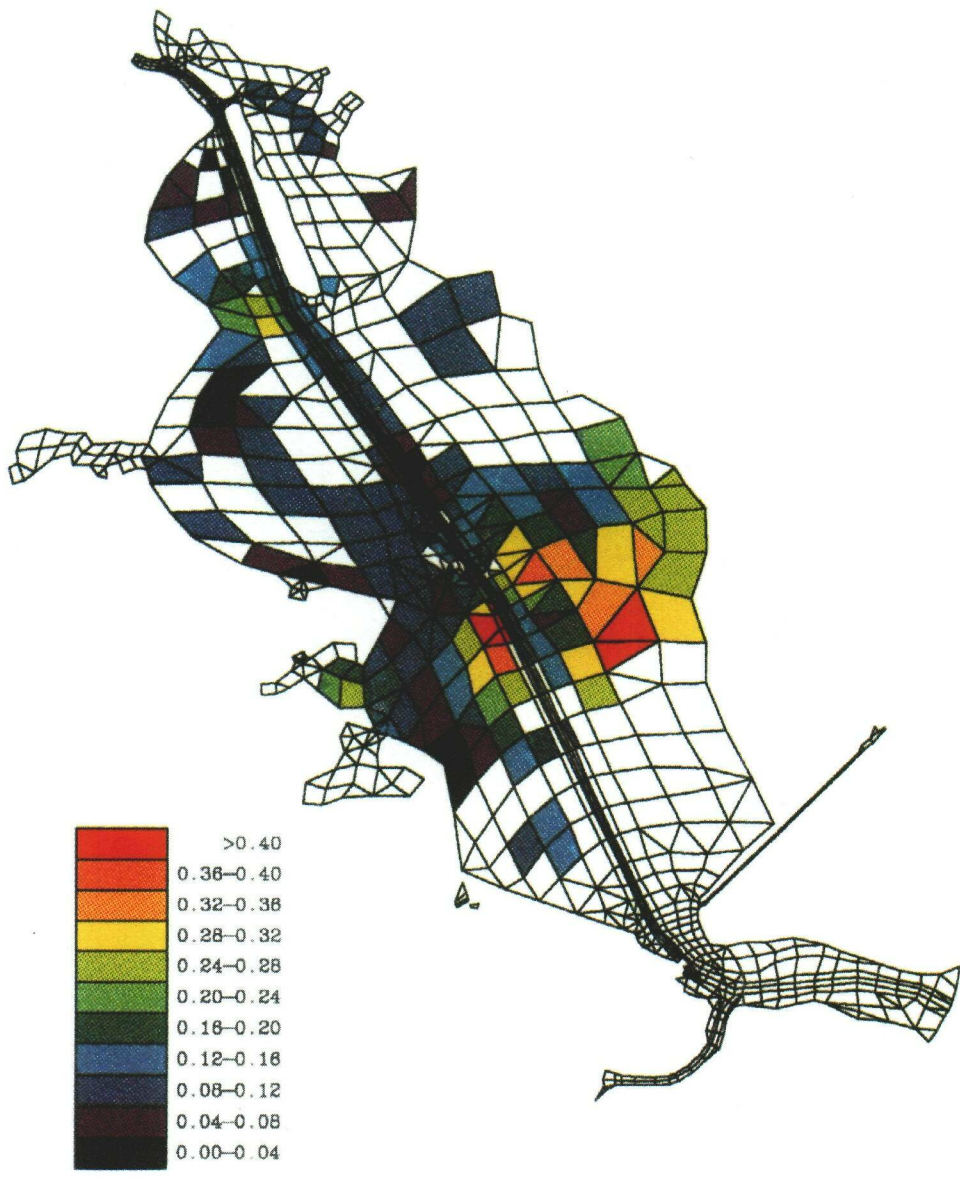


Figure 15 – Continued

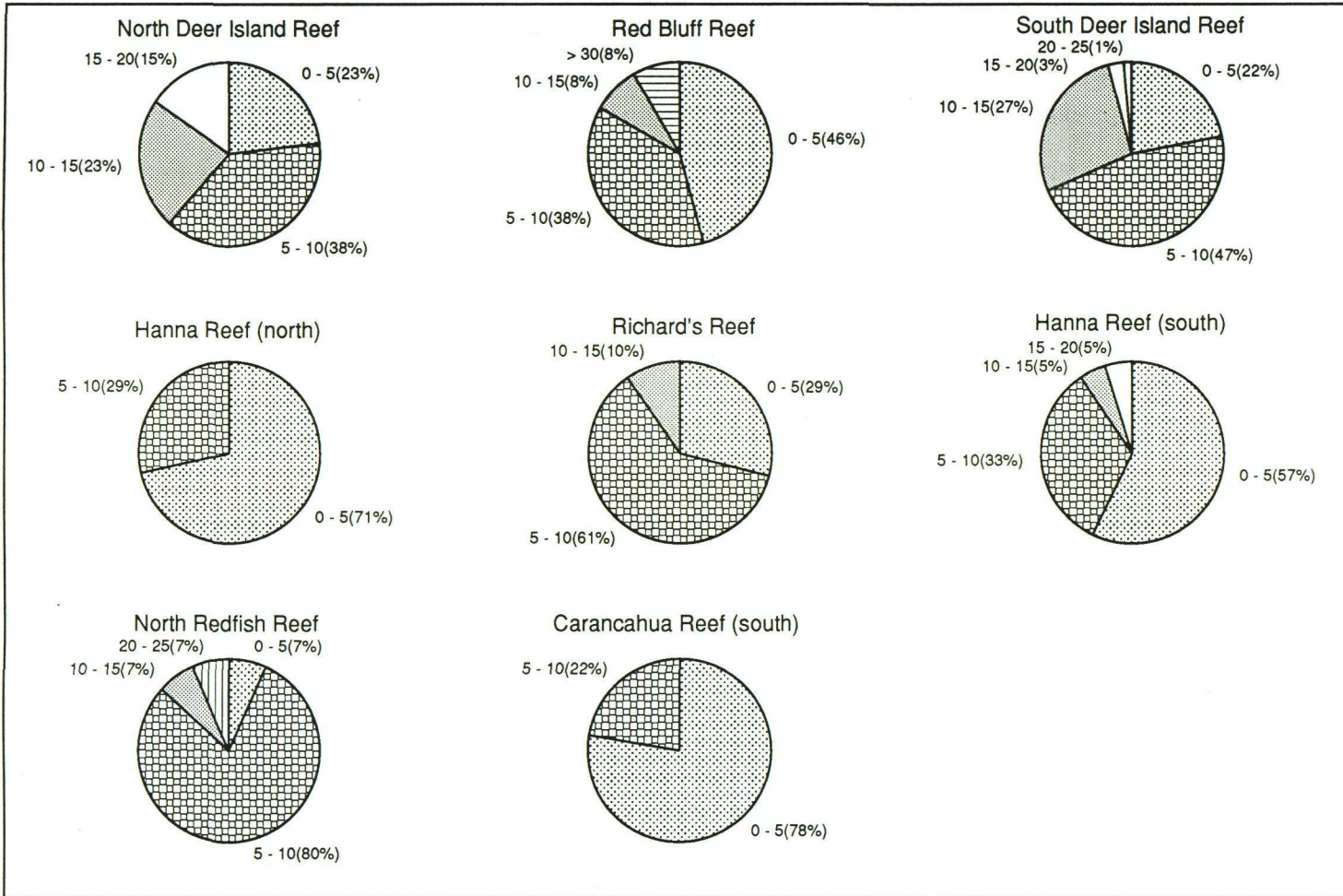


Figure 16. Plots of carapace width size-frequency distribution for those sites where crabs were abundant.

Figure 16 – Continued

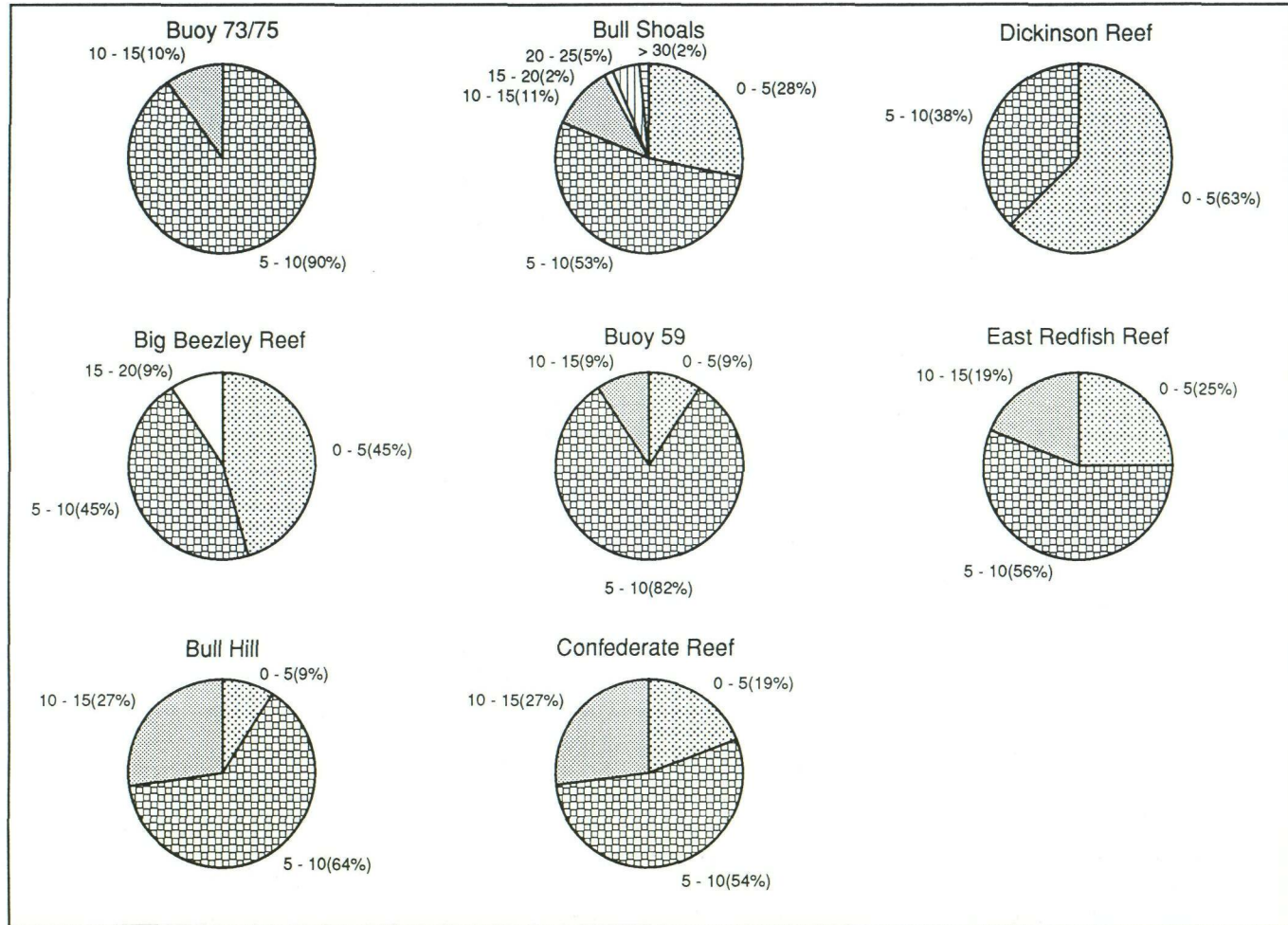


Figure 16 - Continued

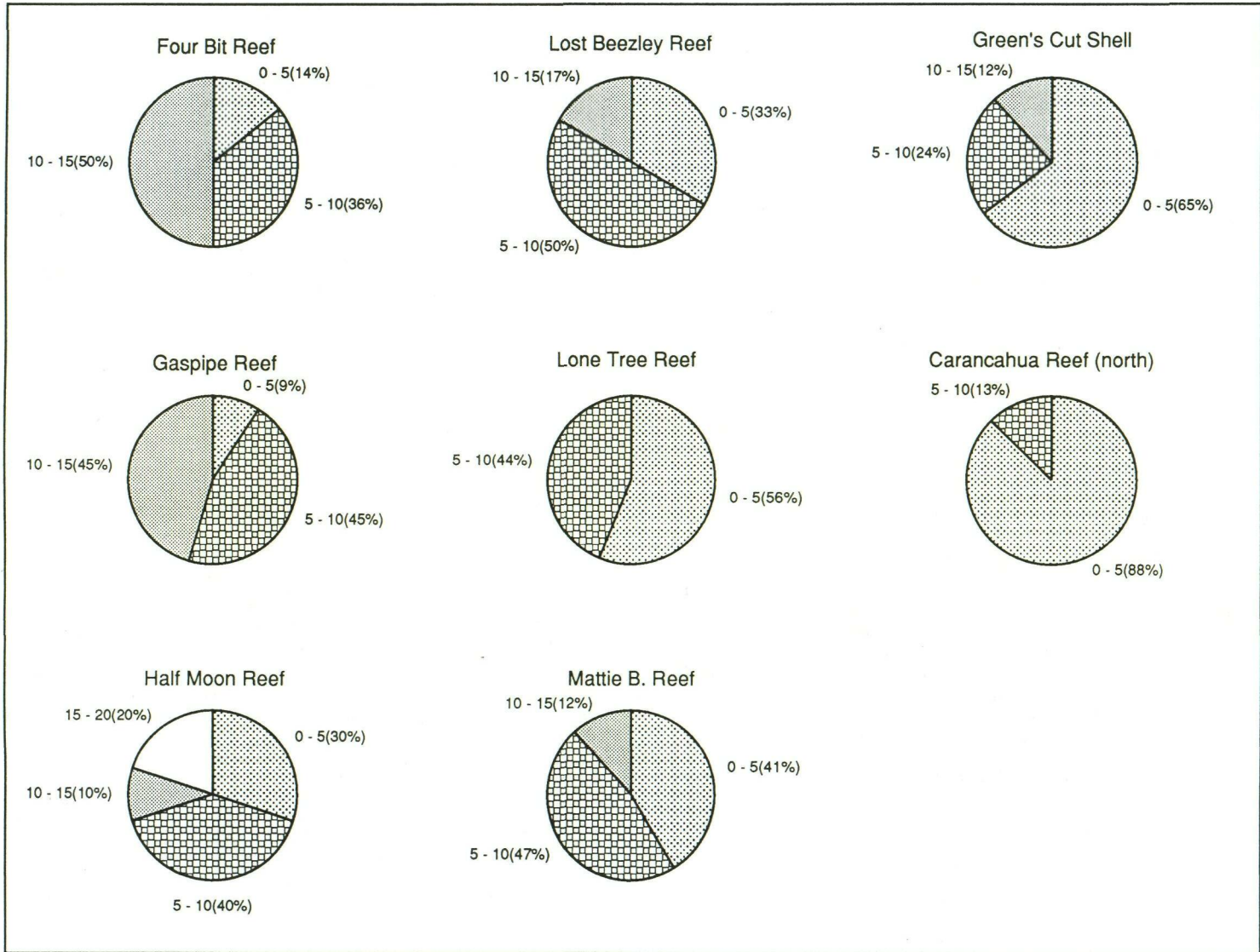
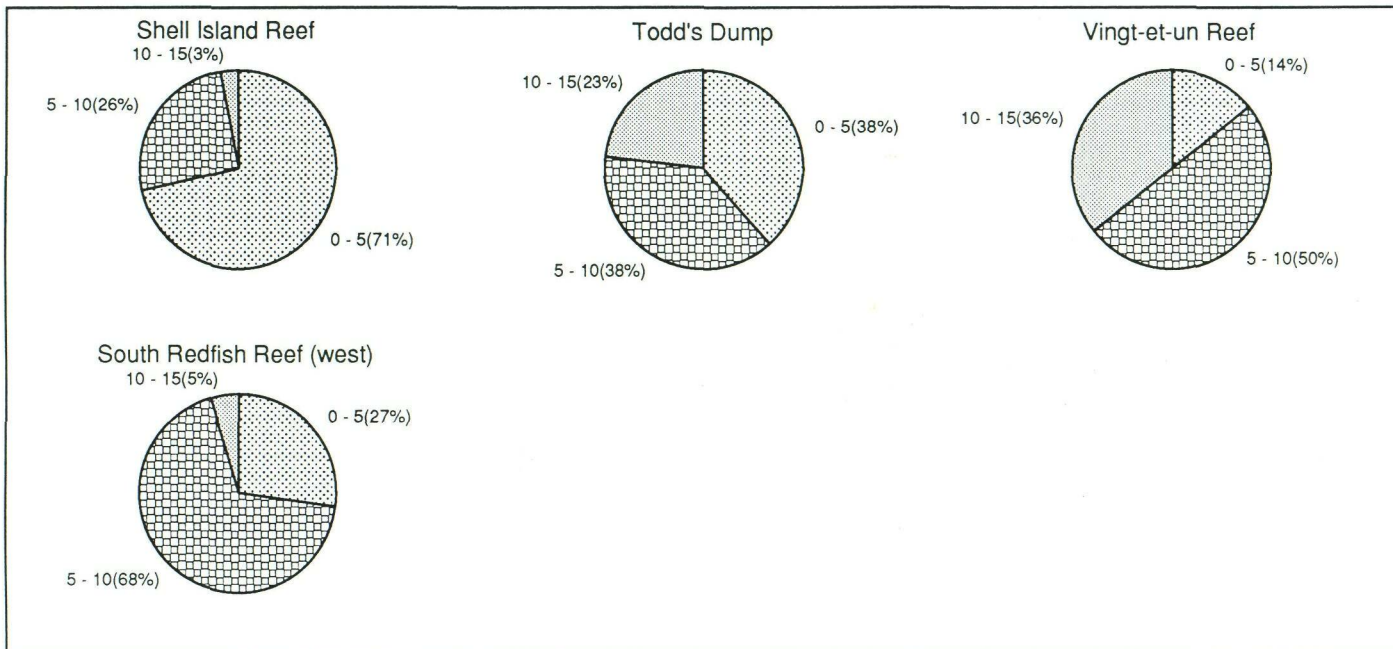


Figure 16 – Continued



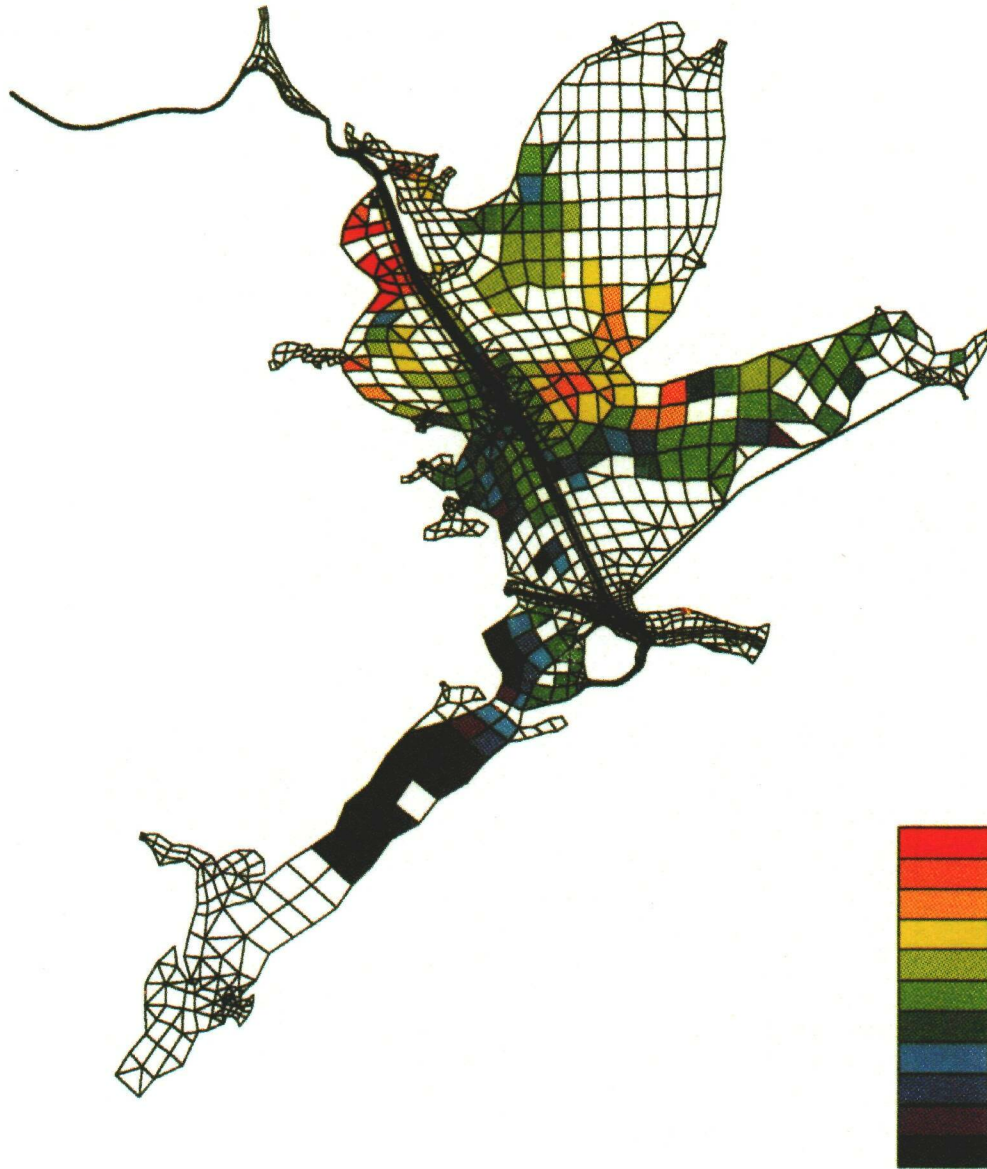


Figure 17. Estimated distribution of mussels (ind m<sup>-2</sup>) obtained using the 51 known sites to predict the values at all unsampled locations and a close-up of the estimated distribution of mussels along the Houston Ship Channel. The grid is the grid of elements used for the Berger et al. (1992) finite element hydrodynamic model of Galveston Bay.

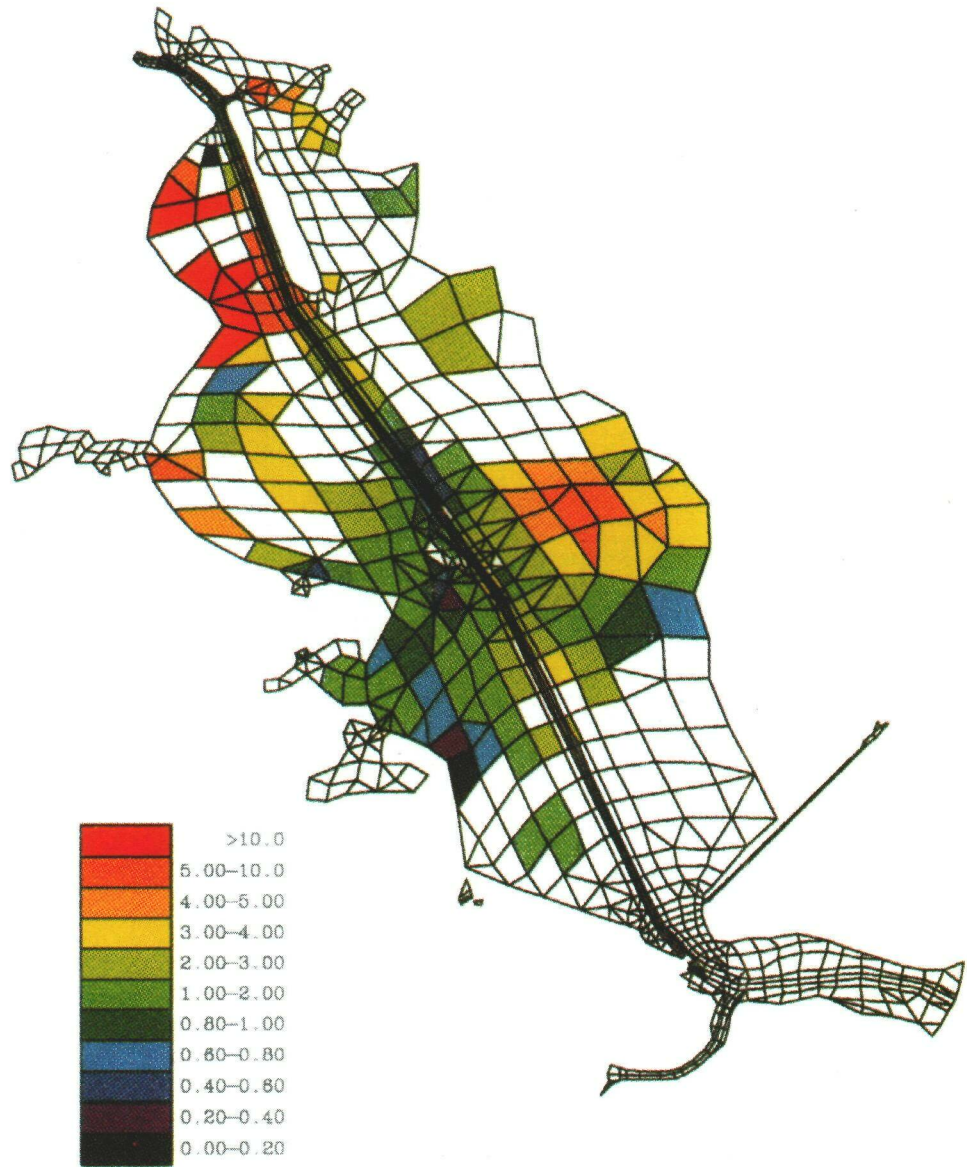


Figure 17 – Continued

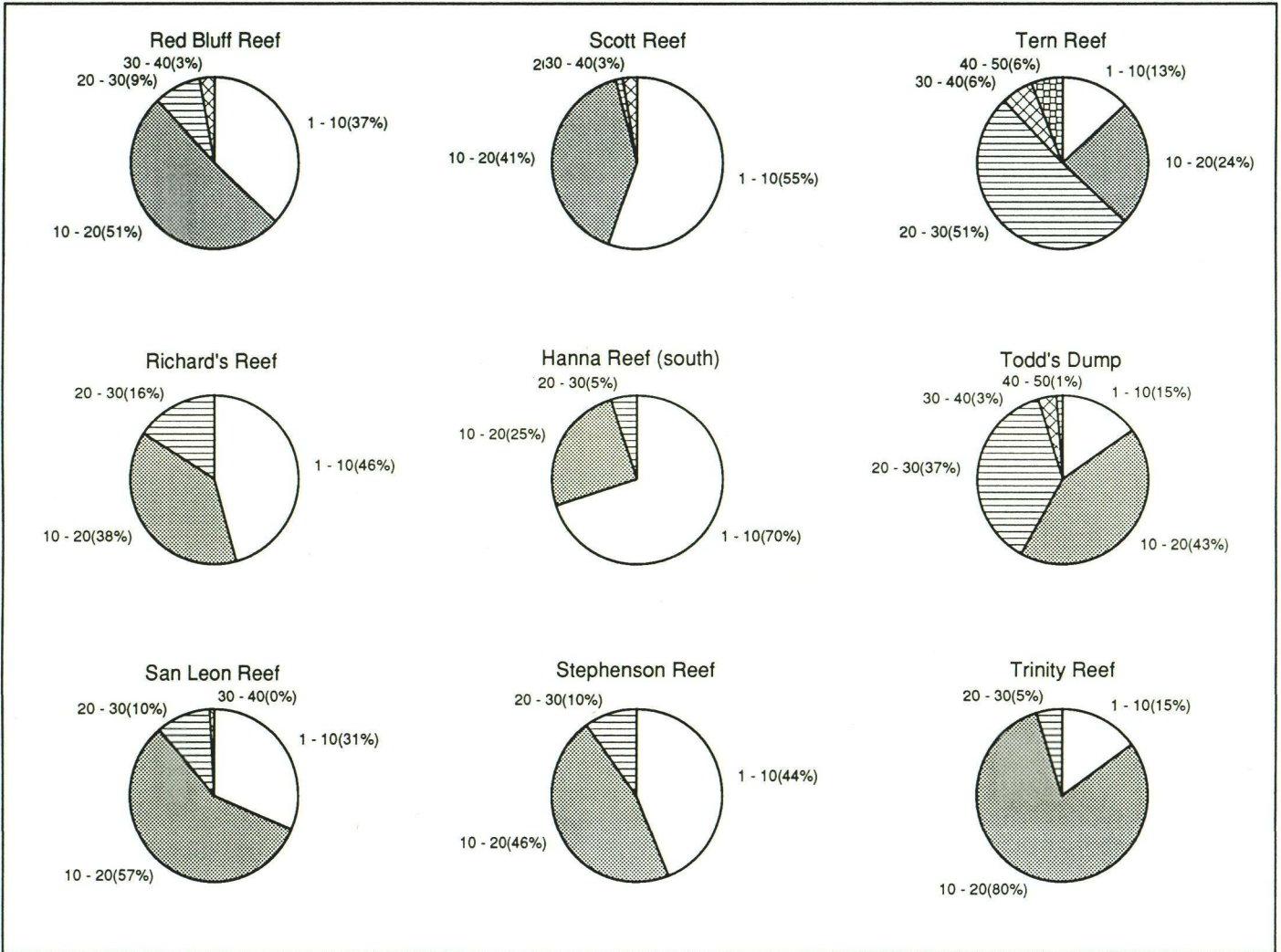


Figure 18. Plots of mussel length size-frequency distribution for those sites where mussels were abundant.

Figure 18 – Continued

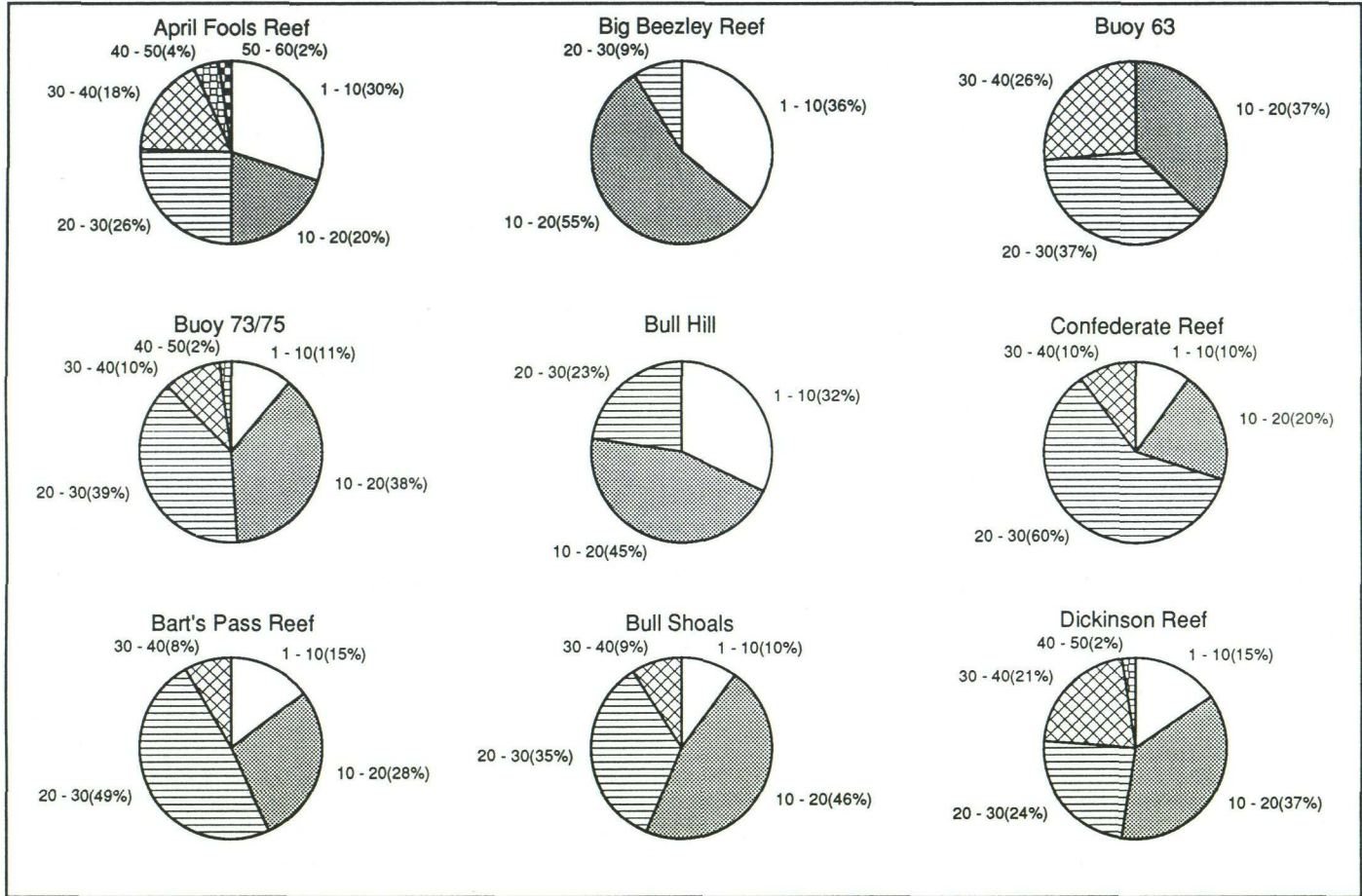


Figure 18 – Continued

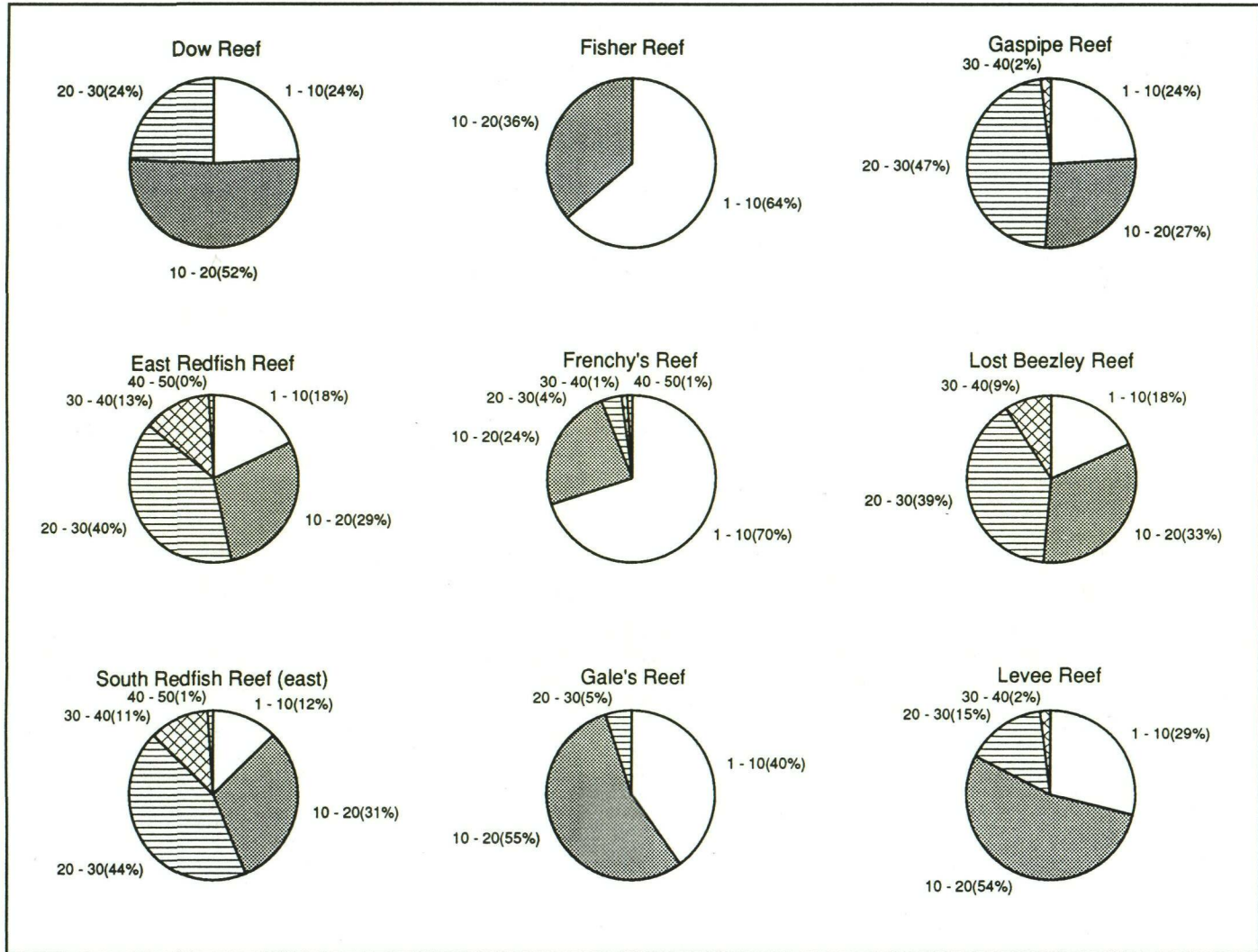


Figure 18 – Continued

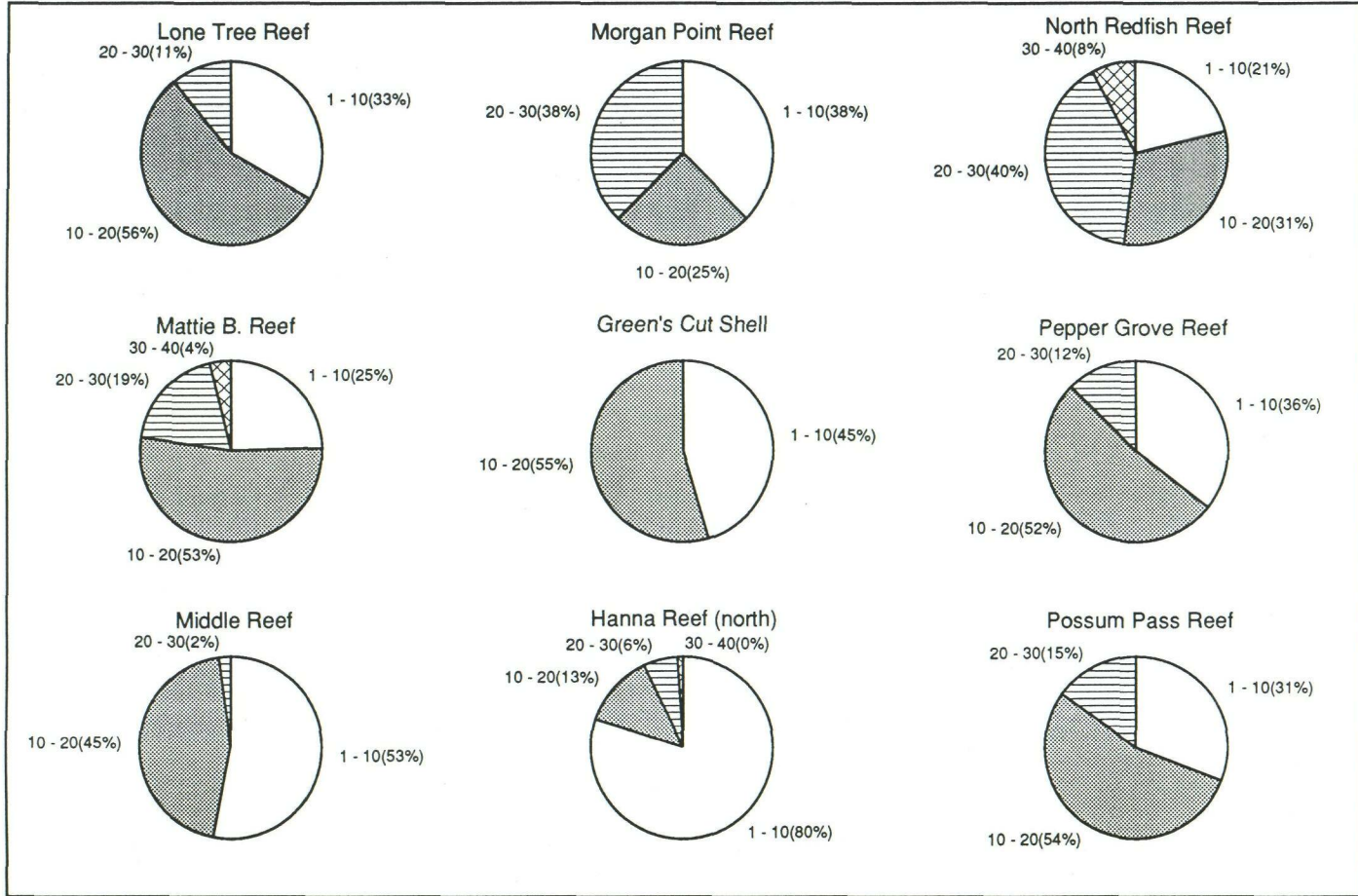
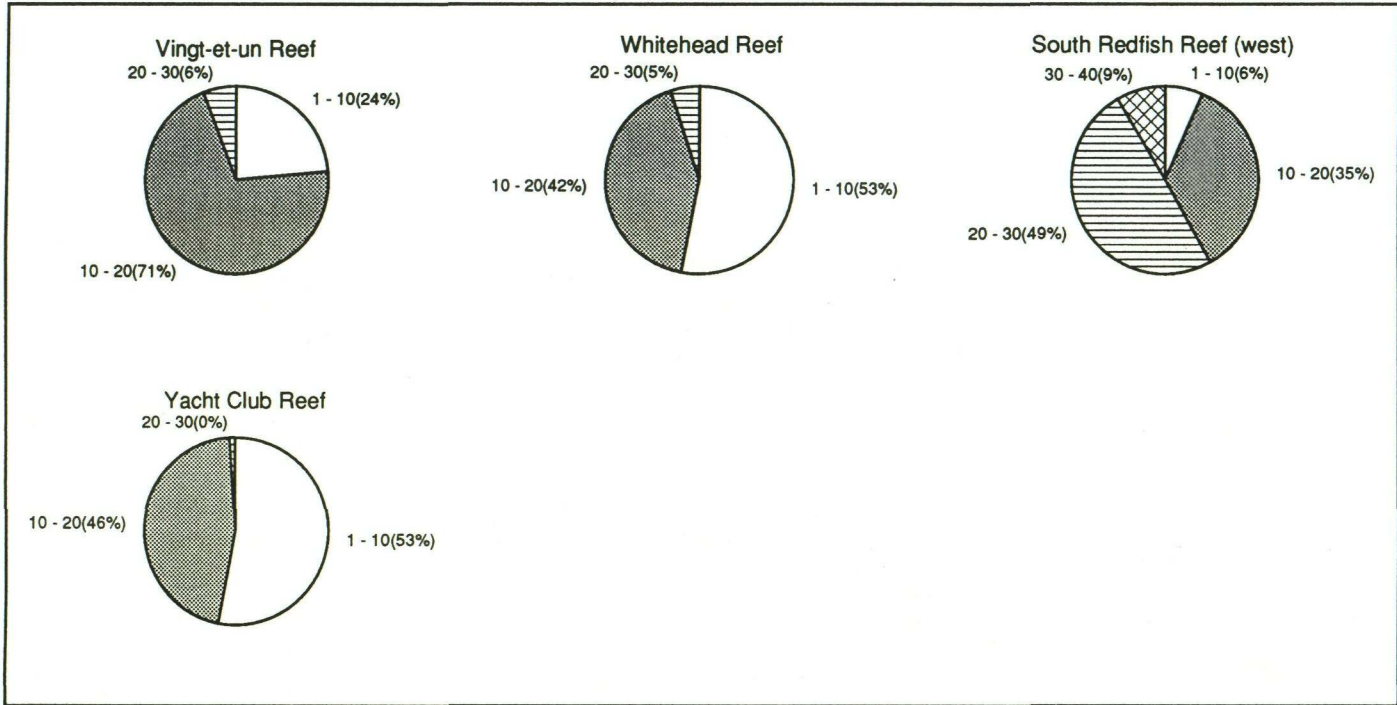


Figure 18 – Continued



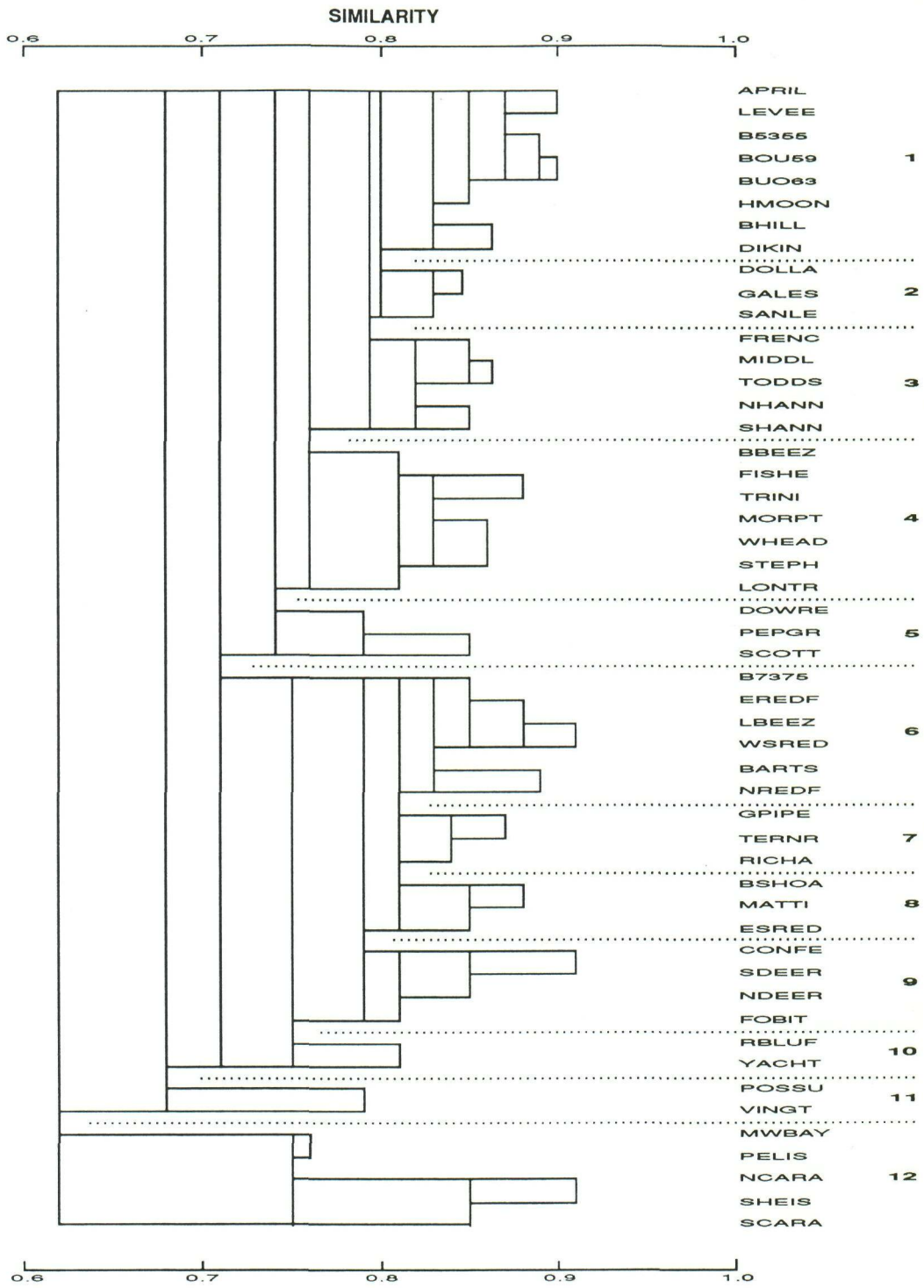


Figure 19. Cluster diagram for the variables normalized and standardized as described in the Methods section.

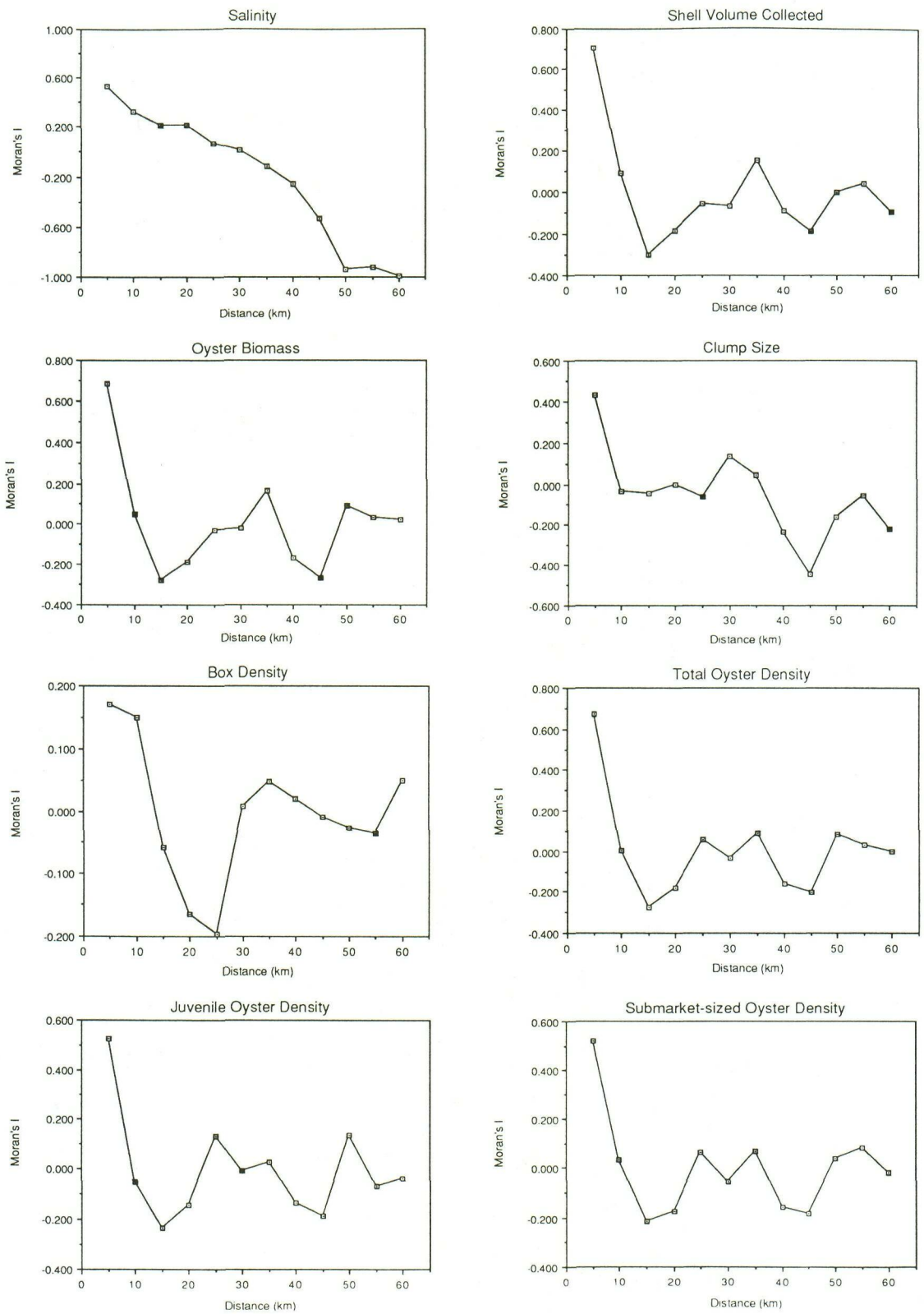
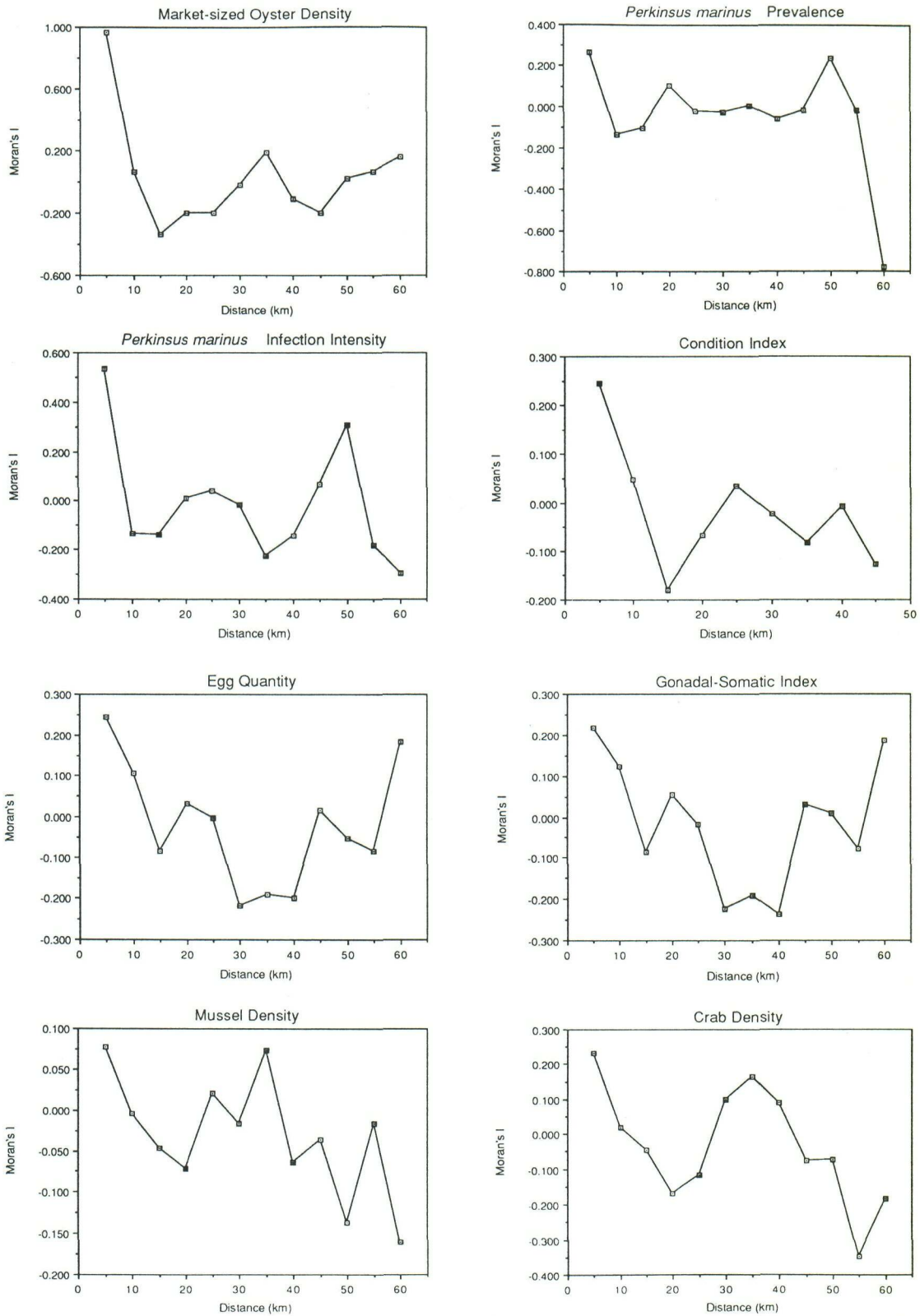


Figure 20. Correlograms of Moran's I versus distance along the Gabriel network (Figure 2).



1-2

Figure 20 – Continued

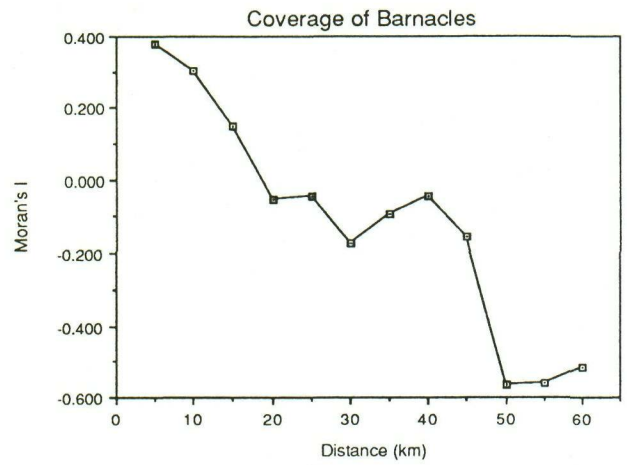
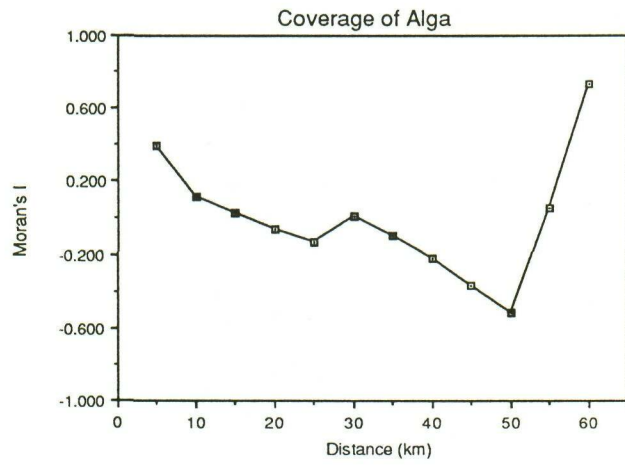
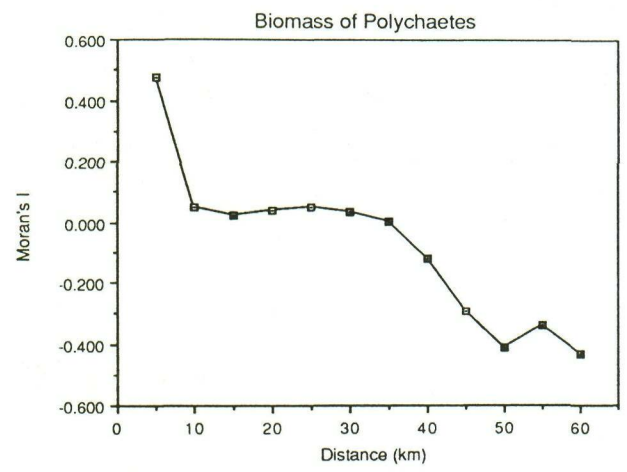
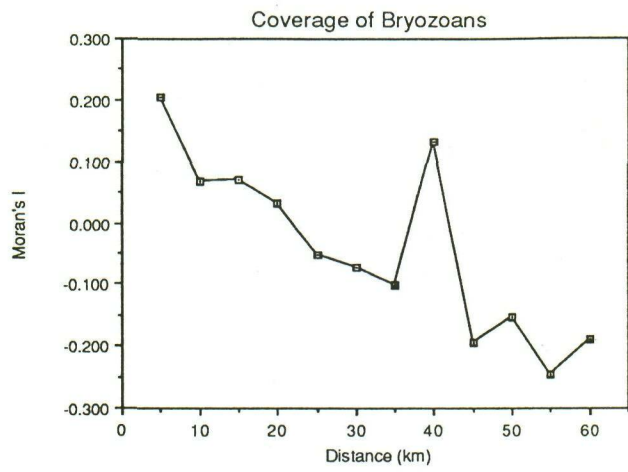


Figure 20 – Continued

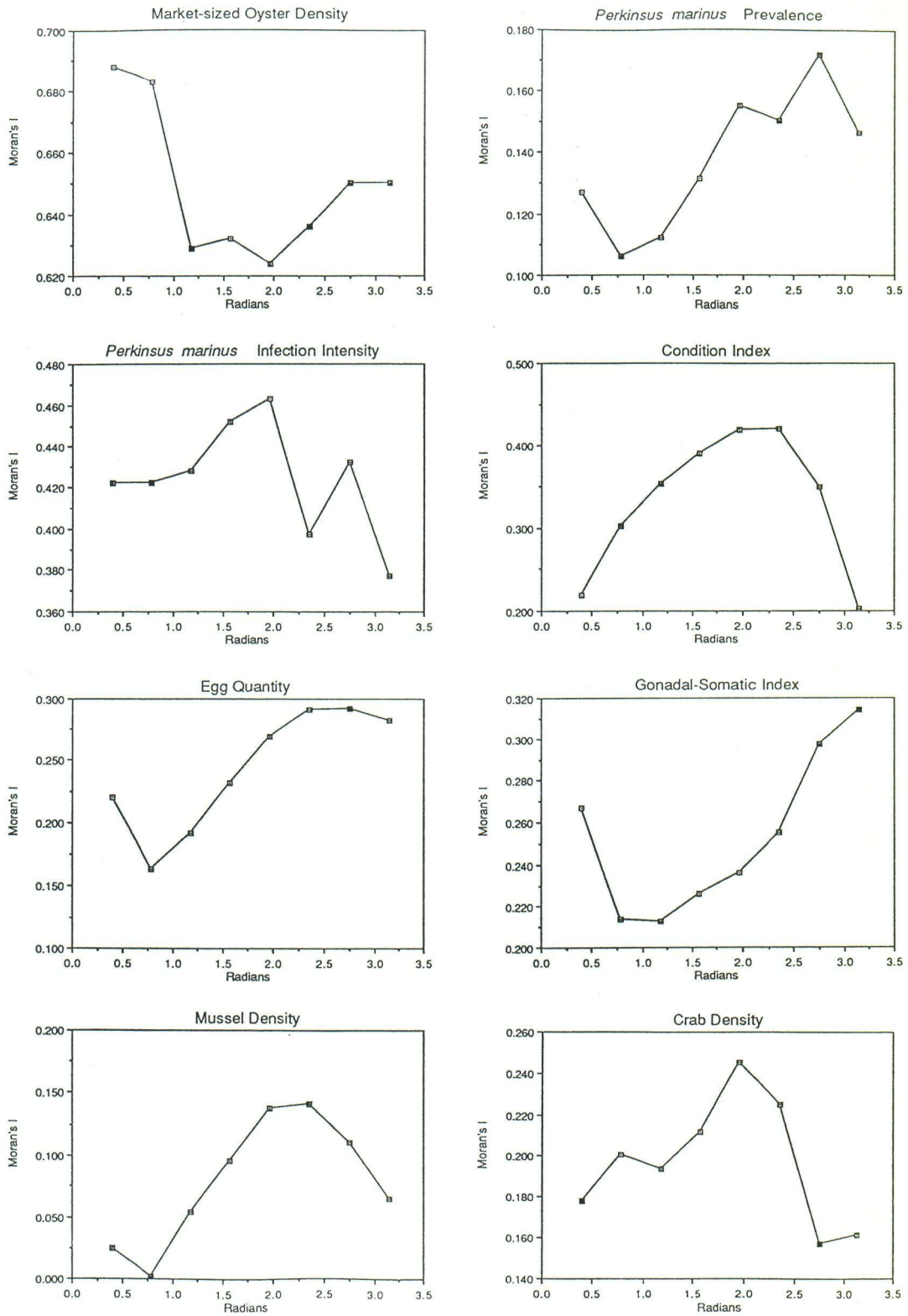


Figure 21. Correlogram of Moran's I versus compass direction computed with respect to the Gabriel network (Figure 2). Divisions of X-axis in radians correspond to a clockwise sweep from NNE/SSW (22.5°) through E/W (90°) to S/N (180°).

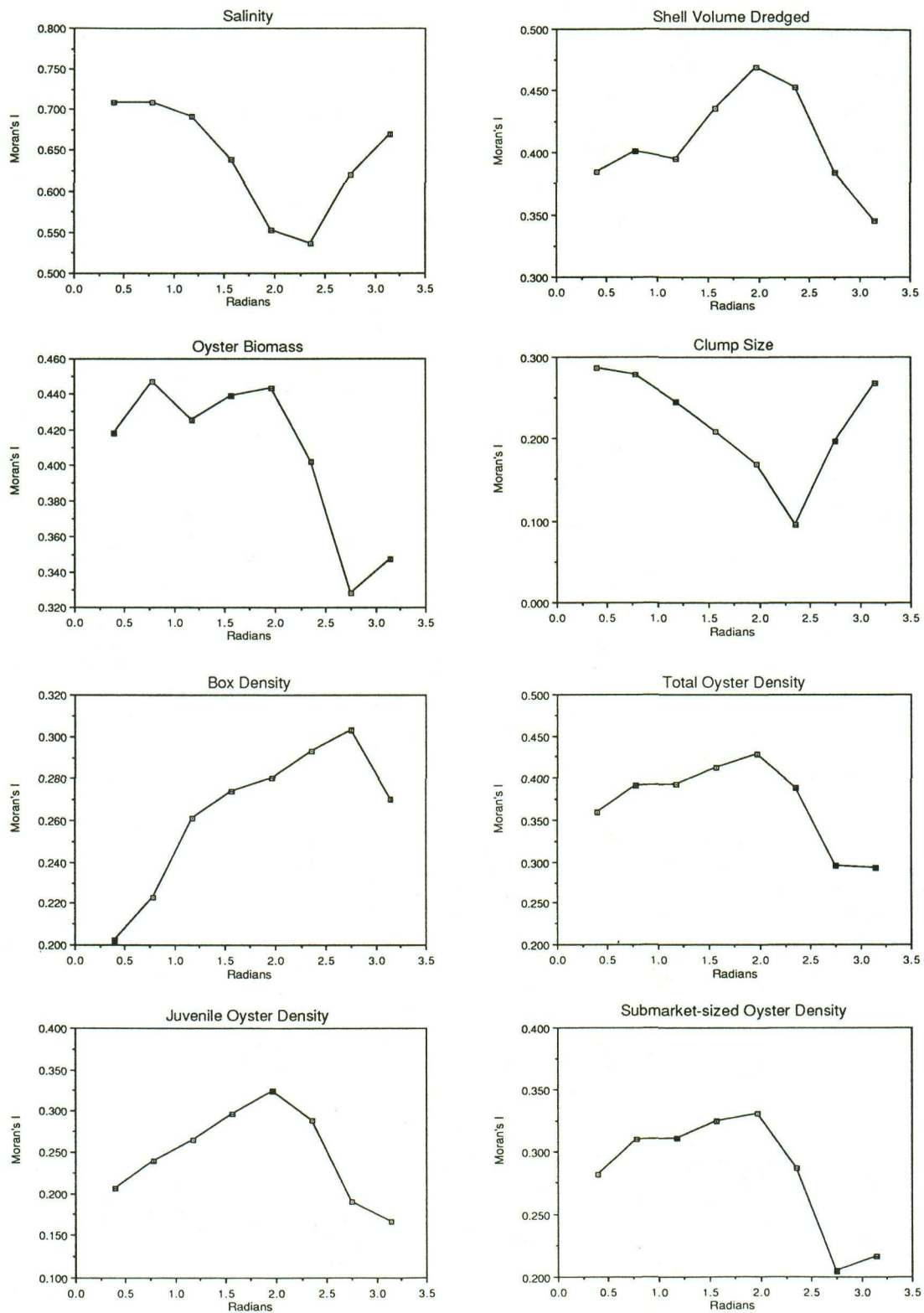


Figure 21 – Continued

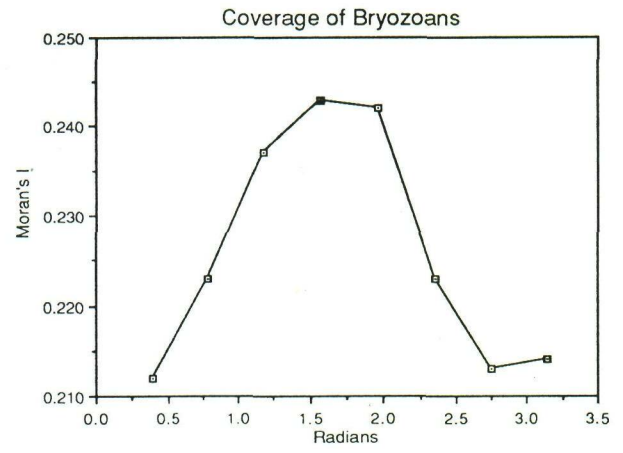
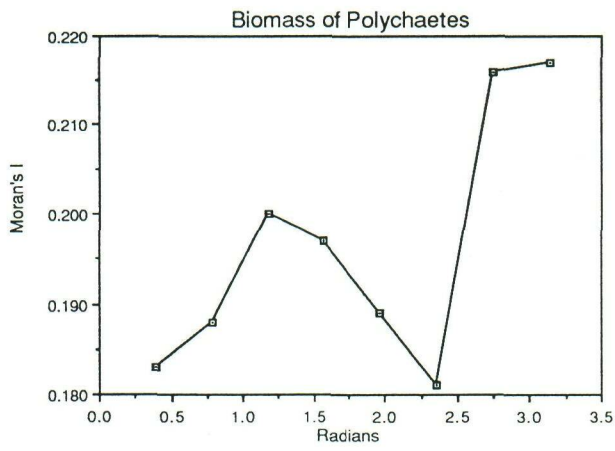
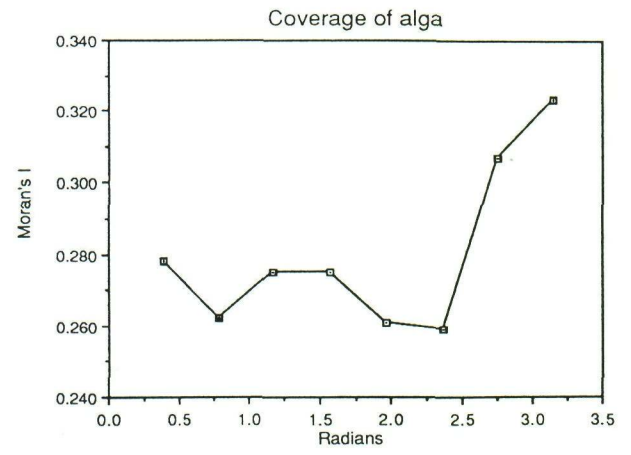
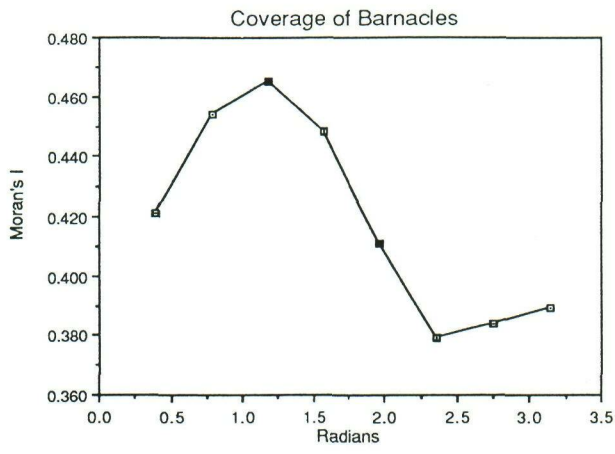


Figure 21 – Continued

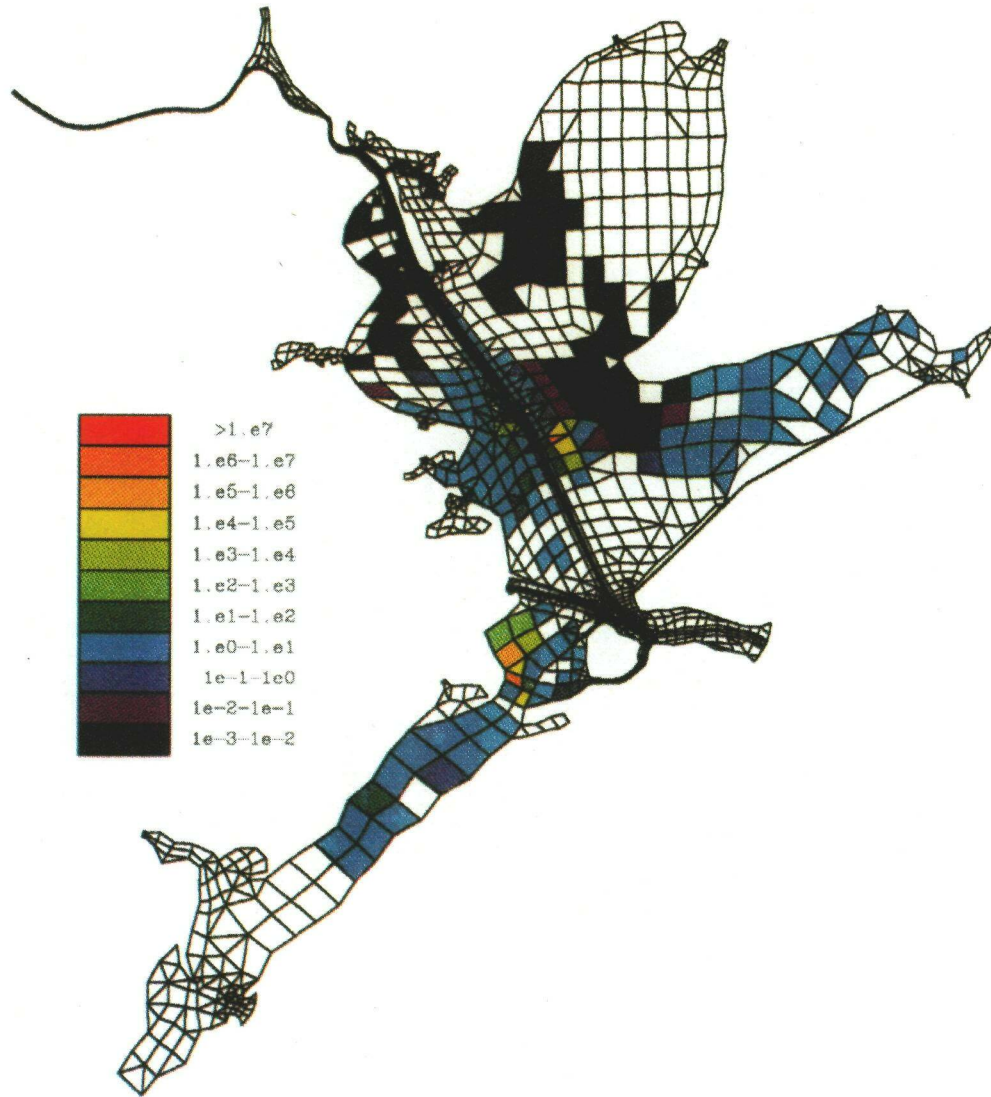


Figure 22. Oyster abundance (ind m<sup>-2</sup>) in December of year two for simulated oyster populations exposed to monthly mean freshwater inflows and temperatures for an average year, the resulting current flow and salinity structure predicted by the Berger et al. (1992) finite element hydrodynamic model of Galveston Bay, and the predator and competitor abundances measured in this study.

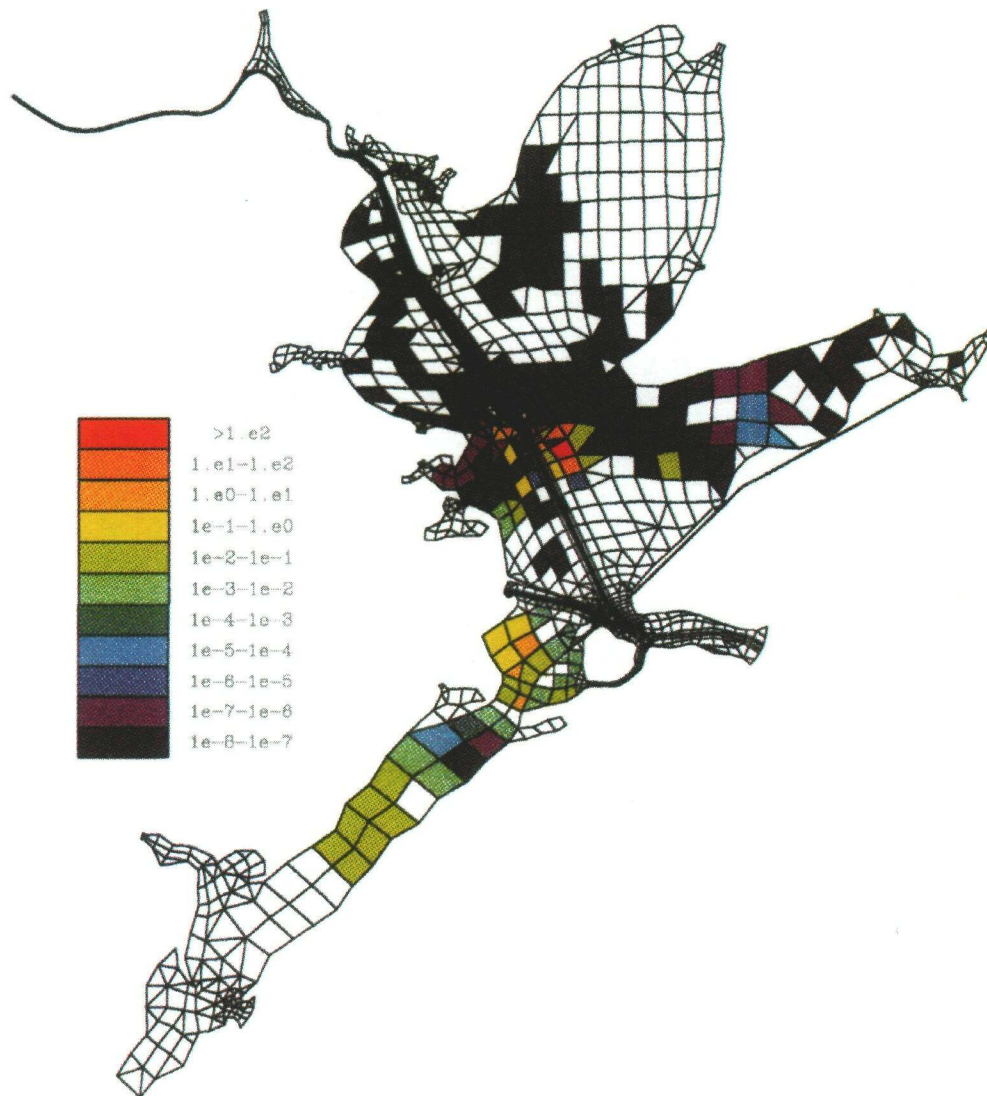


Figure 23. Adult oyster abundance (ind  $m^{-2}$ ) in December of year two for simulated oyster populations exposed to monthly mean freshwater inflows and temperatures for an average year, the resulting current flow and salinity structure predicted by the Berger et al. (1992) finite element hydrodynamic model of Galveston Bay, and the predator and competitor abundances measured in this study.

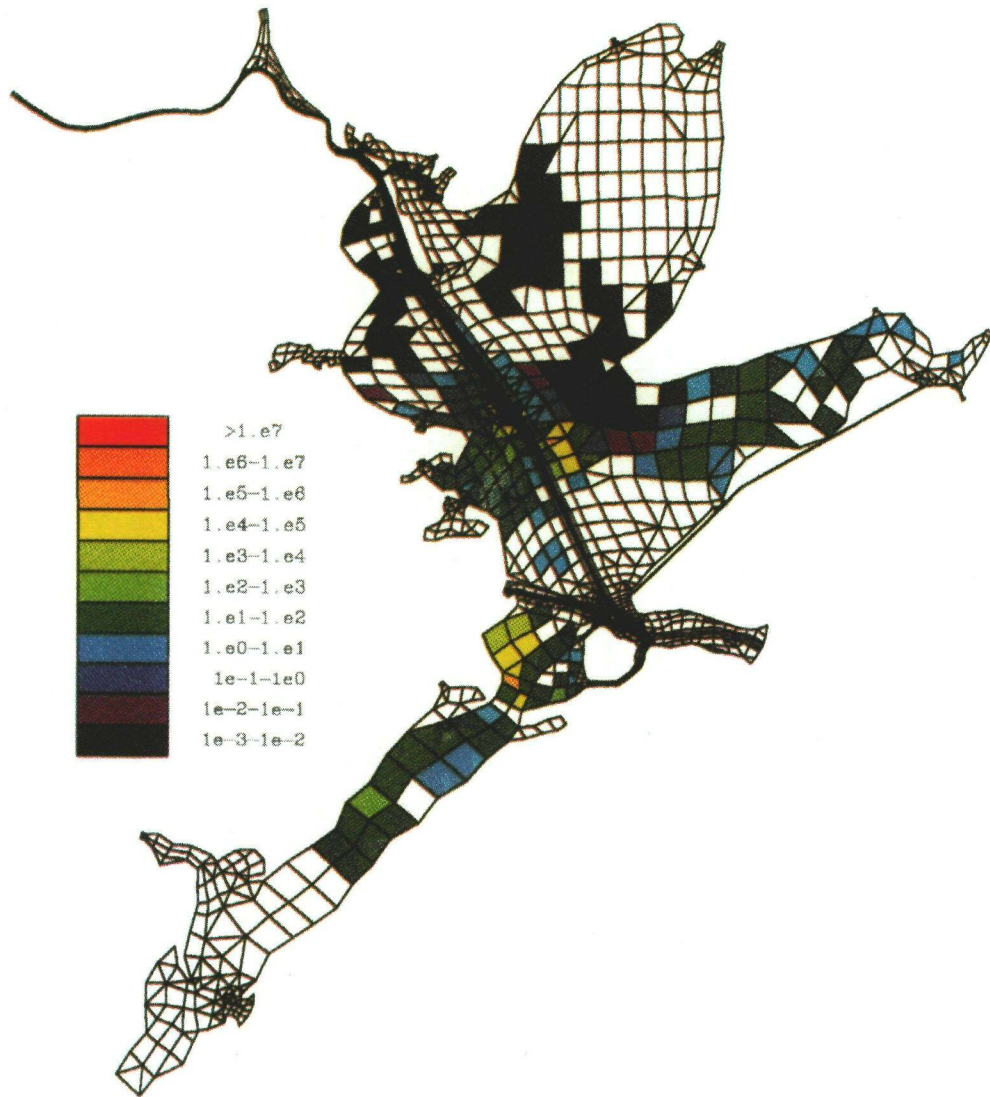


Figure 24. Oyster biomass ( $\text{lb ft}^{-2}$ ) in December of year two for simulated oyster populations exposed to monthly mean freshwater inflows and temperatures for an average year, the resulting current flow and salinity structure predicted by the Berger et al. (1992) finite element hydrodynamic model of Galveston Bay, and the predator and competitor abundances measured in this study.

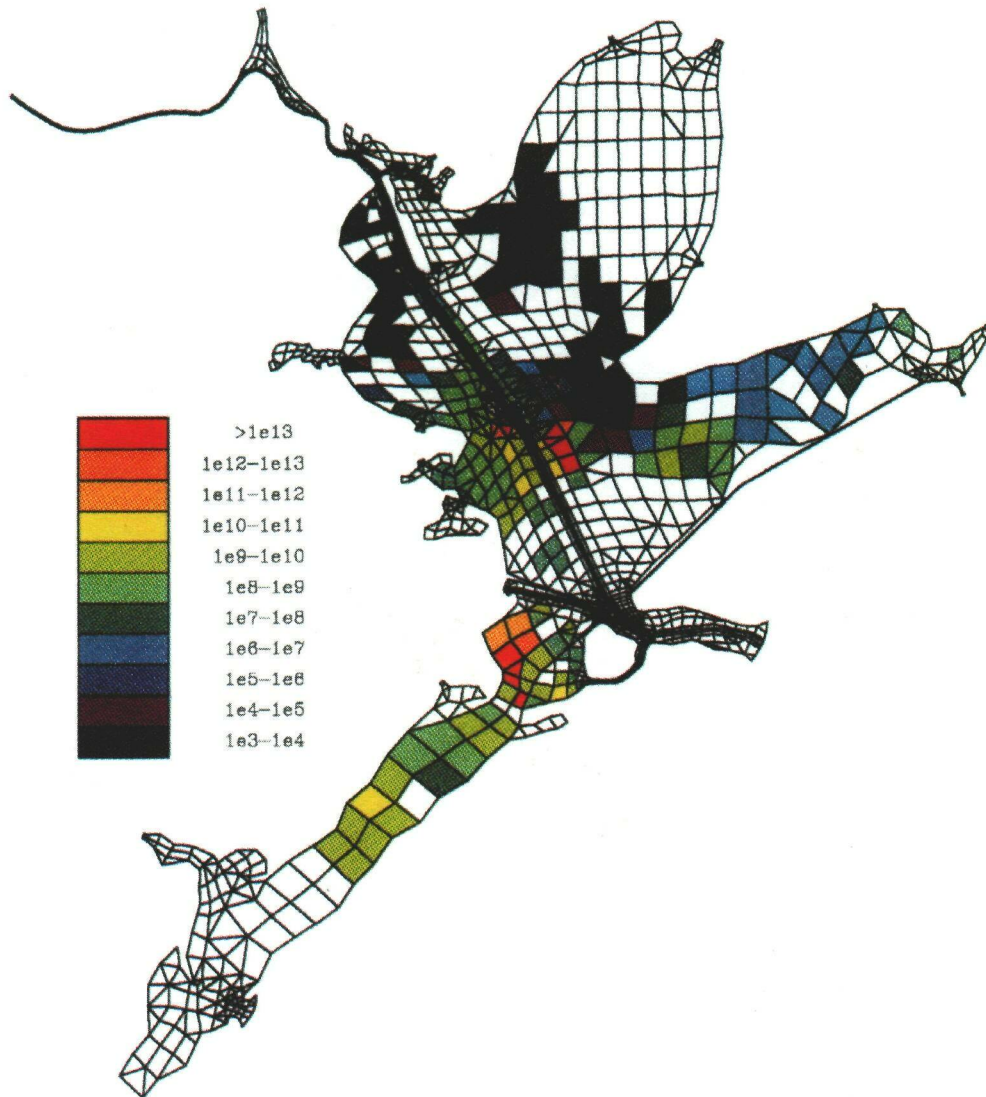


Figure 25. The number of eggs produced (eggs m<sup>-2</sup>) during year two for simulated oyster populations exposed to monthly mean freshwater inflows and temperatures for an average year, the resulting current flow and salinity structure predicted by the Berger et al. (1992) finite element hydrodynamic model of Galveston Bay, and the predator and competitor abundances measured in this study.

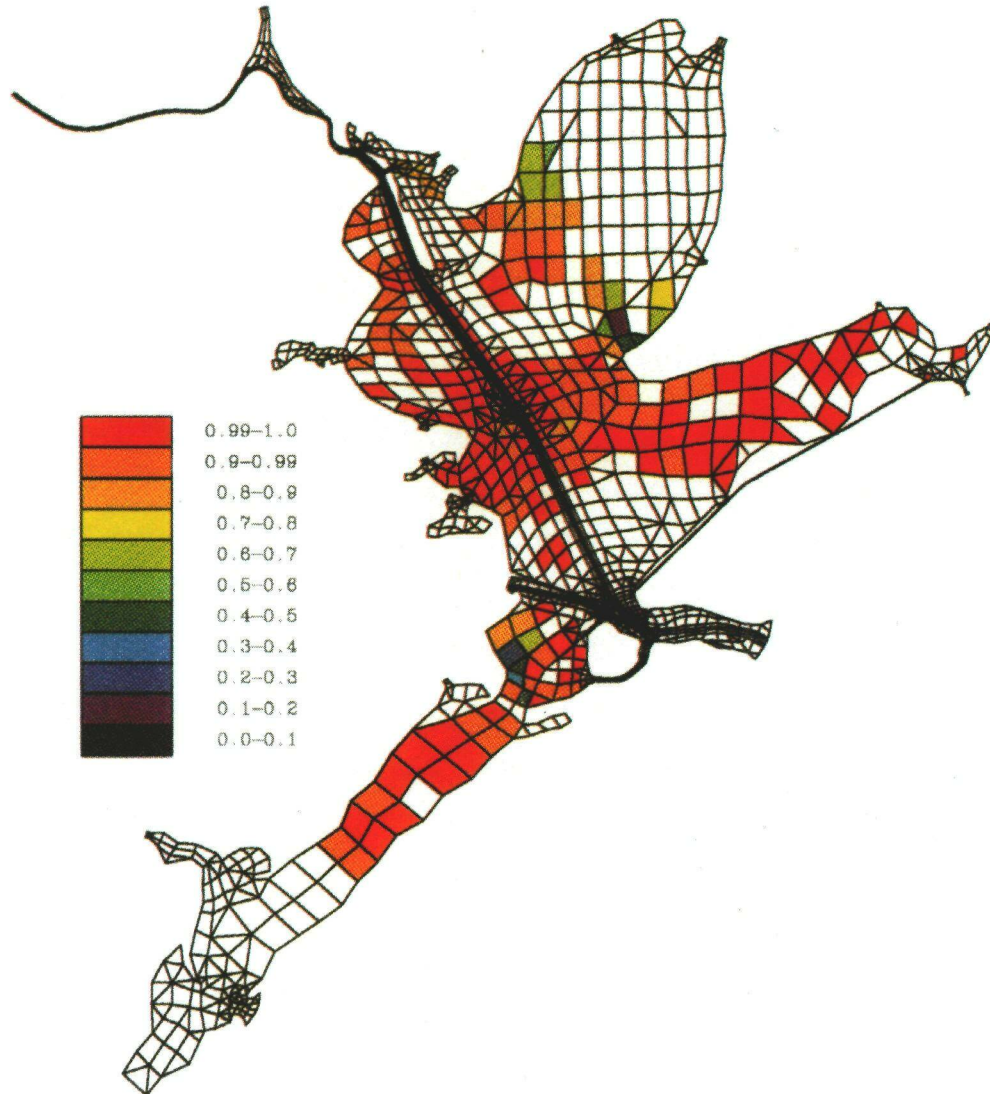


Figure 26. *Perkinsus marinus* prevalence in August of year two for simulated oyster populations (A) and the market-size component (B) exposed to monthly mean freshwater inflows and temperatures for an average year, the resulting current flow and salinity structure predicted by the Berger et al. (1992) finite element hydrodynamic model of Galveston Bay, and the predator and competitor abundances measured in this study.

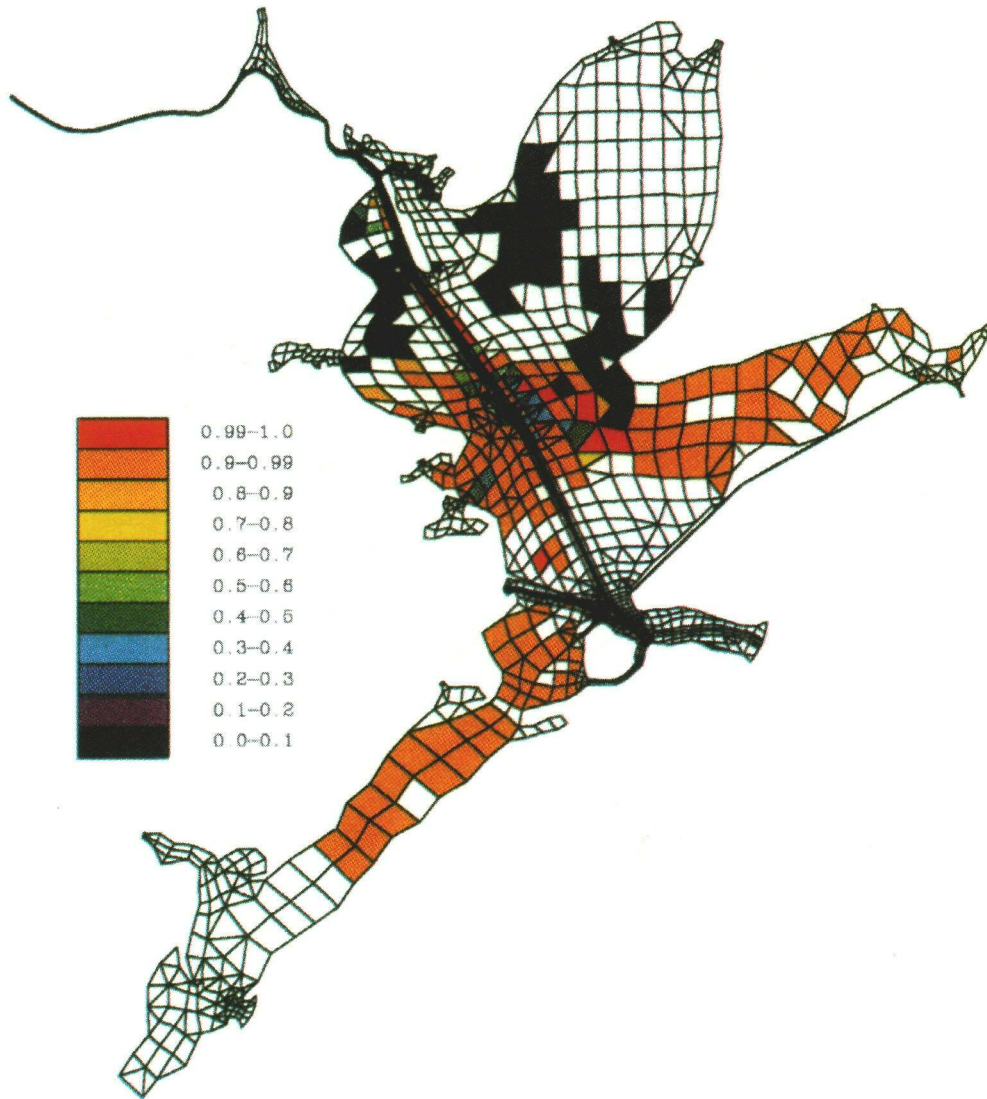


Figure 26 – Continued

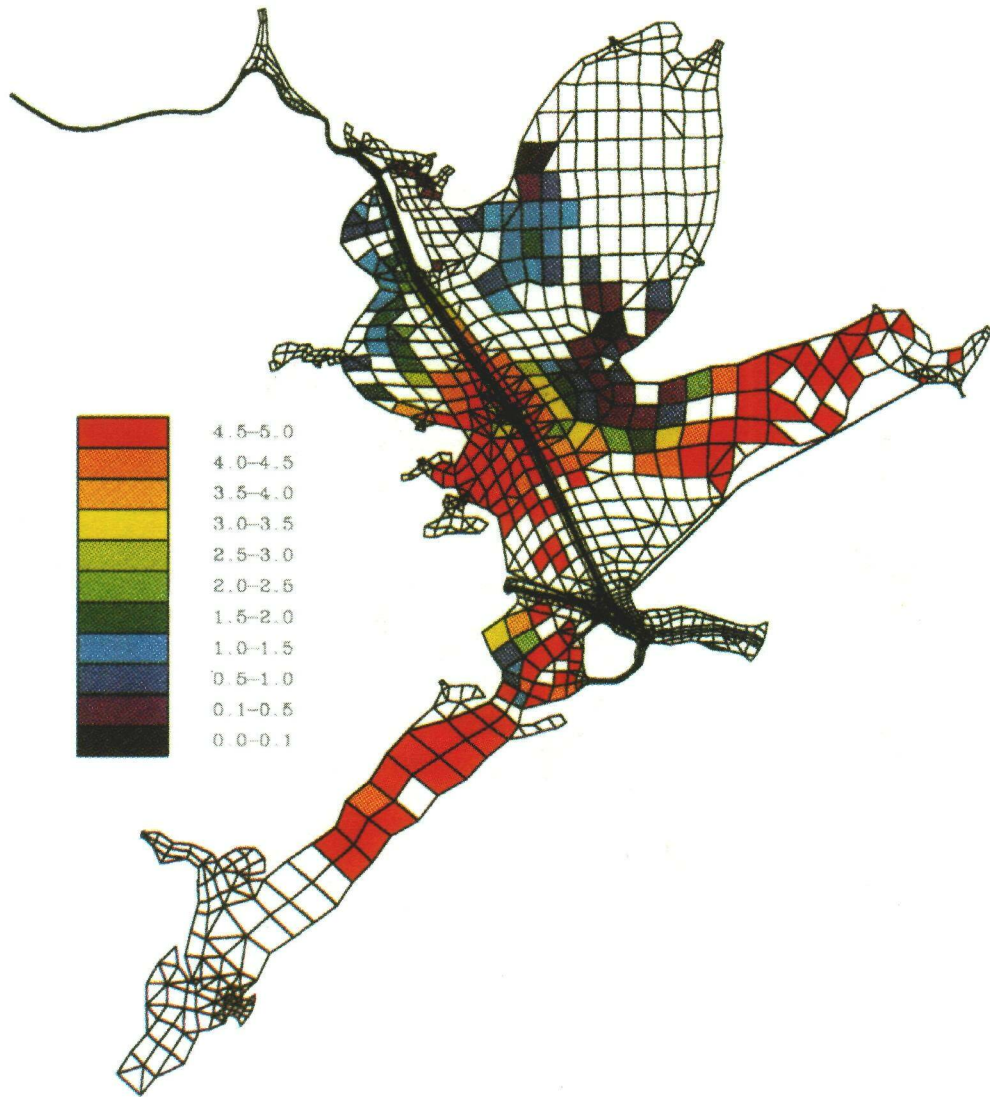


Figure 27. *Perkinsus marinus* infection intensity (Mackin's units) in August of year two for simulated oyster populations (A) and the market-size component (B) exposed to monthly mean freshwater inflows and temperatures for an average year, the resulting current flow and salinity structure predicted by the Berger et al. (1992) finite element hydrodynamic model of Galveston Bay, and the predator and competitor abundance measured in this study.

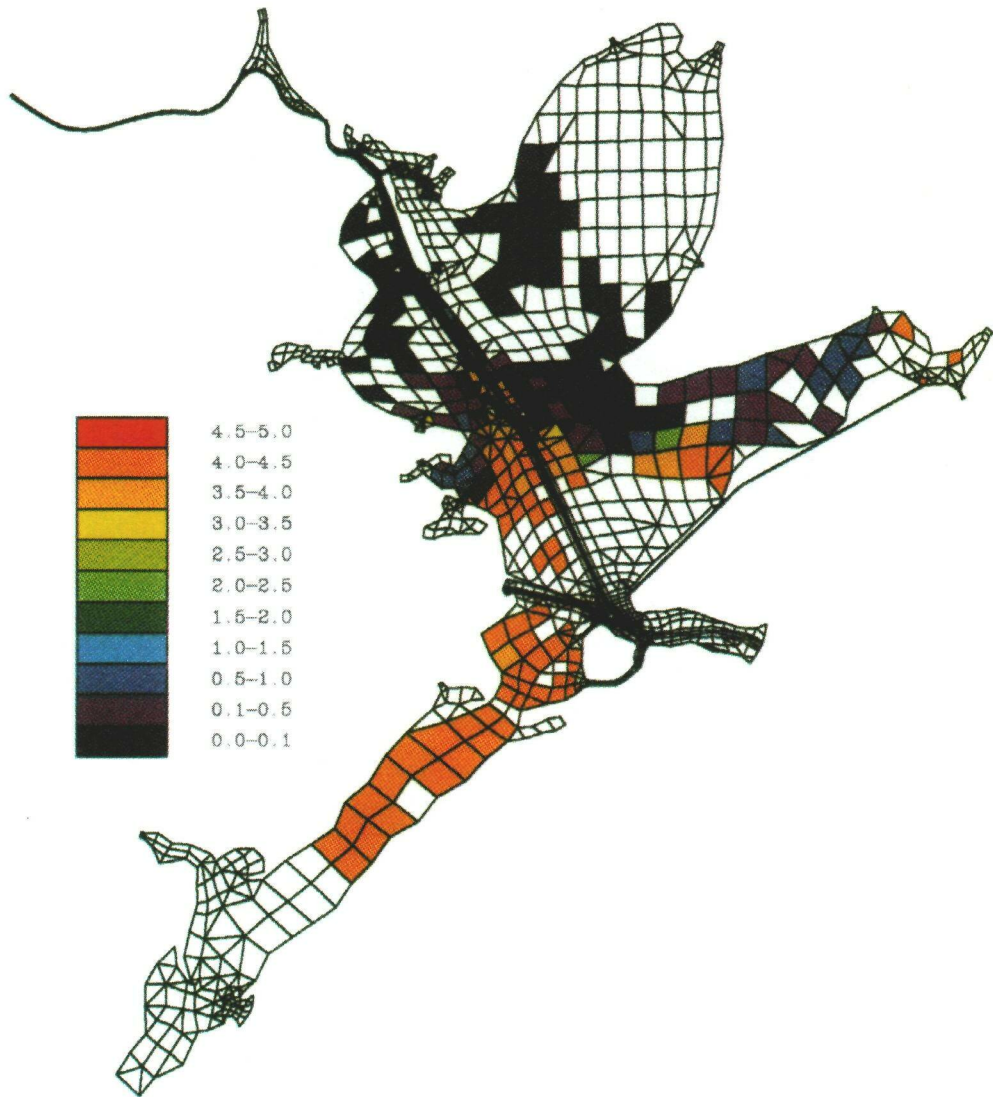


Figure 27 – Continued